Infiltration into a Uniform Sand Column with a Central, Small and Cylindrical Space Filled with a Coarser Sand

By Yasuo ISHIHARA, Eiichi SHIMOJIMA and Yujin MINOBE

(Manuscript received June 12, 1987)

Abstract

This paper deals with an investigation on the confined infiltration process of rainwater into a heterogeneous field that consists of a uniform sand column (outer domain) which centrally contains a vertical, small coarser sand cylinder (inner domain) connected to the surface of the column. Attention is paid especially to the effect of pore-air on the infiltration.

At first, in order to examine the effect of the existence of the inner domain and its depth on the infiltration, an infiltration experiment under ponding and constant-flux conditions is carried out by changing the kind of sand of the inner domain, i. e., the diameter of sand, and the diameter and depth of the inner domain, where the sand used is initially air-dry. During the experiment, water content, pore-air pressure at the bottom of the sand column and infiltration rate are measured. Next, the experimental result is discussed by using the fundamental equation of movement of water and pore-air and referring to the result on the infiltration into a homogeneous sand column already clarified in our previous research. Finally, the effect of the heterogeneity due to the existence of the inner domain in a homogeneous field on ponded infiltrtation is clarifed by considering the developing condition of a quasi-saturated zone formed from the sand surface downward and the situation of escape of pore-air into atmosphere.

1. Introduction

Infiltration field of rainwater is usually not uniform either vertically or laterally. Such a heterogeneity is characterized by several lengths. Recently, infiltration into a heterogeneous field has attracted the attention of hydrologists. One aspect is the problem concerning a spatial variability of soil hydraulic properties under a relatively large spatial scale like watershed or hillslope (e. g., Peck (1983)[1]). The other aspect is the problem especially caused by the existence of macropores like fissures in clay or rock, earthworm holes and root channels in soil (e. g., Beven & Germann (1982)[2]).

The research on the former, that is, how to estimate areal mean infiltration rate is undertaken through the statistical representation of a given field based on scaling theory (e. g., Warrick & Nielsen (1980)[3]) and by using a simplified infiltration formula because purely physical water flow analysis may be not practical (e. g., Smith & Hebbert (1979)[4], Sharma & Gander et al (1980)[5], Maller & Sharma (1981, 1984)[6],[7]). On the other hand, the existence of macropores creates a very complicated situation, and also the

A part of the result of this paper has been published in the Pre-Conference Proceedings of International Conference on "Infiltration Development and Application (1987)", pp. 94-103, in Hawaii.

water flow behaviour through macropores and the hydraulic condition on the boundary between macropores and matrix are said not to be clear (see : Beven & Germann[2]). Simultaneously with experimental studies in a given field, fundamental research on the effect of the existence of macropores on infiltration capacity and the water flow in a matrix has also been experimentally and/or theoretically carried out (e.g., Germann & Beven (1981, 1986)[8),9)], Beven & Germann (1981)[10)], Davidson (1984, 1987)[11),12)]). However, although much research on the infiltration into heterogeneous fields has been undertaken, it appears that little attention has been given to the effect of the pore-air in soil on infiltration.

As has already been mentioned by the authors (Ishihara & Shimojima (1983)[13)], Shimojima & Ishihara (1984)[14)]), in the infiltration process of rainwater, the pore-air in soil is replaced by penetrating water and the air escapes from the ground into the atmosphere. Such an effect of pore-airs on the infiltration has been clarified to be important. Therefore, in order to clarify the infiltration process into a heterogeneous field, the role of pore-air in the infiltration process should be explored.

In this paper, a finer sand column with a central vertical coarser sand cylinder connected to the surface of the finer, outer column is taken as an example of such a heterogeneous infiltration field where the heterogeneity exists laterally. By paying attention to the behaviour of pore-air, the effect of the existence of such a heterogeneity and also the effect of the depth of the coarser, inner sand cylinder on the infiltration are experimentally and analytically discussed by comparing the infiltration into a homogeneous field.

2. Apparatus and method of the experiment

By using an acrylate resin cylinder of 18.5 cm inner diameter and 170 cm length with a bottom plate, a uniform sand column of Sand K-7 vertically containing a central, small sand cylinder of Sand K-5 or Sand K-6, connected to the surface of the outer sand column, was made. Sand K-7 is finer than Sand K-5 and Sand K-6, as shown in **Fig. 1.** The sands employed were initially air-dried. The coarser sand cylinder is about

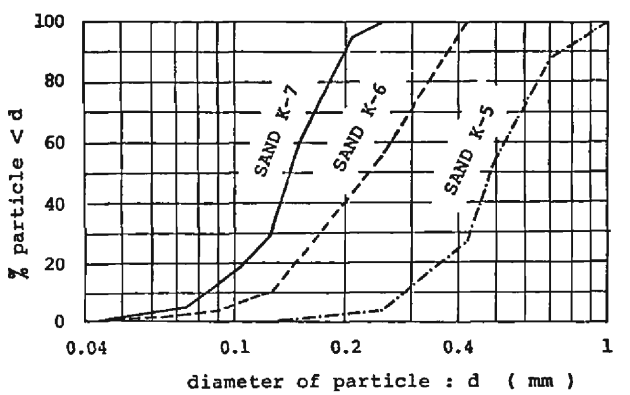

Fig. 1 Particle-size distribution.

1 cm or about 2.7 cm in diameter. The depth to the surface of the finer sand column from the upper edge of the acrylate cylinder is about 2 cm, excluding a special case. The infiltration field in which the bottom of the coarser sand cylinder reaches the bottom plate and where the sand cylinder does not reach the plate are referred to as "type-I" and "type-II", respectively. The coarser sand cylinder and its surrounding domain of coarser sand are called "inner and outer domains" in the infiltration field, respectively.

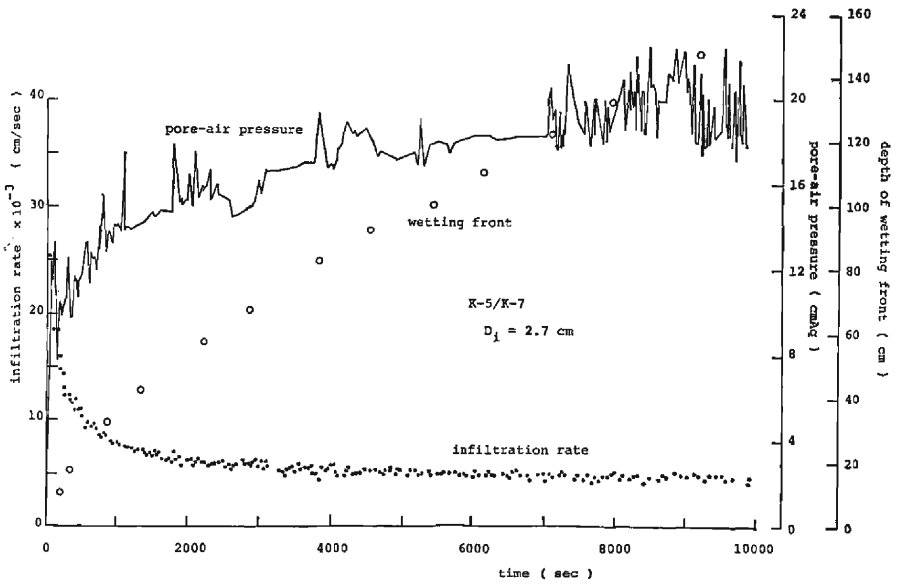

(1) D_i=2.7 cm, h_w=2 cm and K-5/K-7.

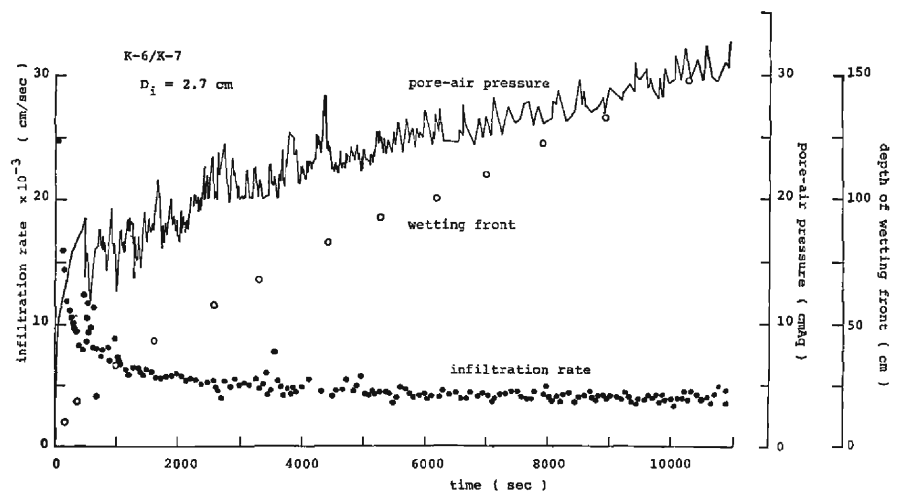

(2) D_i=2.7 cm, h_w=2 cm and K-6/K-7.

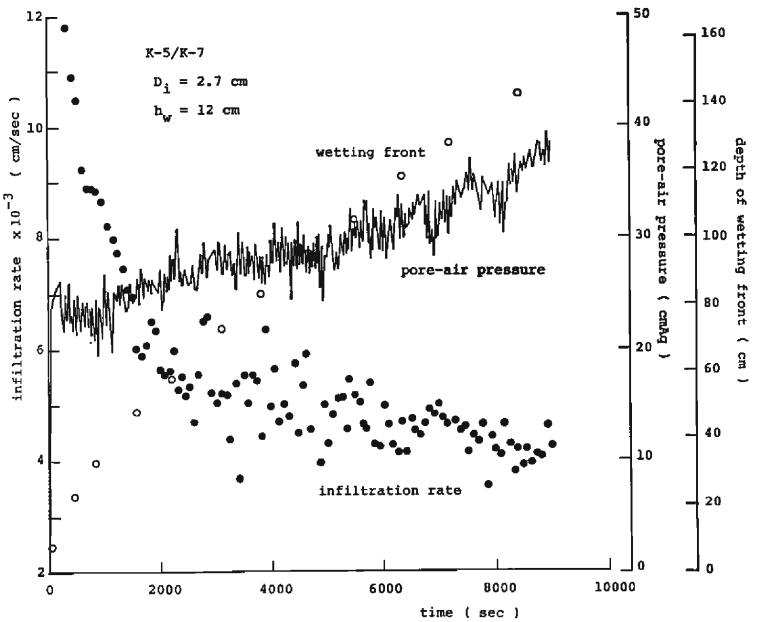

(3) D_i=2.7 cm, h_w=12 cm and K-5/K-7.

Fig. 2 Changes of the infiltration rate, the depth of wetting front and the pore-air pressure with time in the ponded infiltration.

The water supply on the surface of the field is either a constant ponding depth or a constant flux of water. In the case of a constant flux condition, after ponding occurs on the surface of the field, the boundary condition on the surface changes to that of ponding. The ponding depth ultimately becomes constant when the ponding water starts to overflow the edge of the acrylate cylinder. We call the infiltration under the ponding condition and the flux condition as "ponded infiltration" and "flux infiltration", respectively. For the simplification of expression, let us describe the infiltration field employing Sand K-5 and Sand K-6 as "K-5/K-7" and "K-6/K-7", respectively.

The measurements made during the experiments were water content, infiltration rate

Table 1 Experimental condition and characteristic

Exp-I	Sand of inner domain	D_i (cm)	σ (cm^2/cm^2) $\times10^{-2}$	h_w (cm)	f_∞ (cm/sec) $\times10^{-3}$	ω_* (cm/sec) $\times10^{-2}$
(1)	K-5	1	0.29	2	4.0	1.2
(2)	K-6	1	0.29	2	3.9	0.97
(3)	K-5	2.7	2.1	2	4.7	1.2
(4)	K-6	2.7	2.1	2	4.1	1.1
(5)	K-5	2.7	2.1	12	4.3	1.1
homogeneous layer					3.5	0.95

and pore-air pressure. Water content was measured as an average of cross-sectional area of the field by using an electric capacitance method at 13 measuring points at various depths[13]. Infiltration rate was estimated by subtracting the rate of overflowing water from the rate of water supply to make a constant ponding depth over the sand surface. Pore-air pressure was measured by a pressure gauge attached at the bottom of the sand column.

Experiments were carried out till the wetting front reached the bottom of the field in an air conditioned room maintained at about 21°C.

3. Ponded infiltration

3.1 Experimental results

(1) Type-I

Four cases of experiments (Exp-I(1)-(5)) were carried out for type-I. The experimental conditions are shown in **Table 1**, where D_i is the diameter of the inner domain, h_w the ponding depth, and σ the ratio of the cross-sectional area of the inner domain to that of the total domain. Exp-I(5) with the condition that the ponding depth is much greater than in other cases was undertaken to examine the effect of ponding depth on the infiltration process. **Fig. 2**(1), (2) and (3) show the changes of infiltration rate, depth of the wetting front and pore-air pressure with time, corresponding to Exp-I(3), (4) and (5), respectively. **Fig. 3** shows the development of water content profile in Exp-I(3), where the saturated mass wetness of Sand K-7 is about 0.31. The infiltration rate and the excess pore-air pressure from atmospheric pressure are denoted by f and p_a, respectively. It is known from these figures and the results of other cases that,

♯1 the infiltration rate decreases with time, and then becomes a constant, f_∞, asymptotically ;

♯2 the velocity of the wetting front, moving downwards through the outer domain, decreases with time, and then becomes a constant, ω_*, asymptotically ;

♯3 the pore-air pressure increases with time, and then its increasing rate becomes constant, $\dot{p}_{a\infty}$, asymptotically ;

quantities in the ponded infiltration (type-I).

$\dot{p}_{a\infty}$ (cmAq/sec) $\times 10^{-3}$	θ_* (cm³/cm³)	f_{cs} (cm/sec) $\times 10^{-3}$	f'_{cs} (cm/sec) $\times 10^{-3}$	$\omega_*^2\theta_*/\dot{p}_{a\infty}$ (cm/sec) $\times 10^{-2}$	$<K_a>_c$ (cm/sec) $\times 10^{-2}$
1.0	0.34	4.0	4.1	4.7	3.5
2.8	0.39		2.3	1.0	2.0
0.35	0.37	4.8	5.0	14.3	15.7
1.1	0.38	4.4	4.4	4.2	4.5
	0.38	4.8			
2.0	0.37				

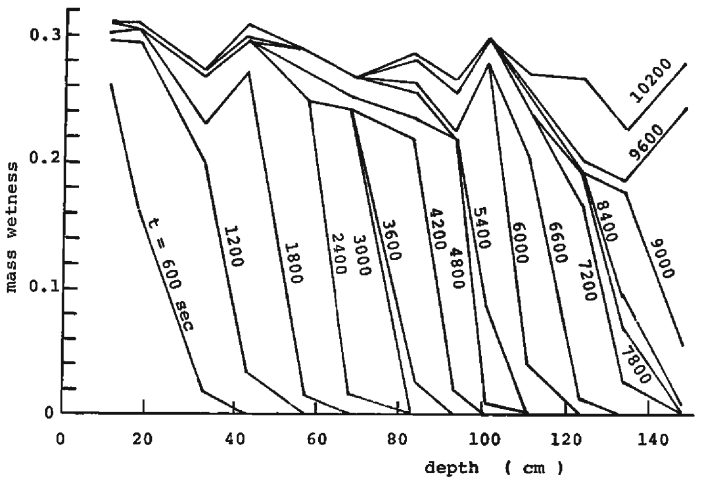

Fig. 3 Development of the profile of water content with time.

♯4 as time goes by, the profile of water content is, in order of depth, composed of the nearly saturated zone referred to "the quasi-saturated zone"[13] which develops downwards from the sand surface. This is followed by the transmission zone with a relatively low but a fairly constant water content, θ_*, and finally the wetting front. Now, we denote the zones excluding the quasi-saturated zone as "the unsaturated zone". The situation, mentioned in ♯1, where the main developing field of the wetting front is the outer domain is known from the wetness degree of profile of water content as shown in **Fig. 3** or the supplementary experiment shown in the **Appendix** or an analysis on the experiment result shown later.

The estimated values of f_∞, ω_*, $\dot{p}_{a\infty}$ and θ_* are summarized in **Table 1**, where the results estimated for the ponded infiltration[13] into a homogeneous sand column of Sand K-7 are, for comparison, shown in the lowest column. Let us designate f_∞ "the ultimate infiltration rate".

From the detailed observation of the situation of air escape from the sand surface during experiments, the following is known:

♯5 The escape of pore-air does not occur just after the beginning of experiment, but then it does occur from the surface of the outer domain for a short time. And then the location of the escape changes and the escape intermittently appears only from the surface of the inner domain. For example, in Exp-I(3) shown in **Fig. 2**(1), the time when the escape of pore-air from the outer domain changes to the inner one is about 110 sec.

We can learn the following from the table : As the value of σ and the sand diameter of the inner domain increase, f_∞ and ω_* become large and $\dot{p}_{a\infty}$ inversely small. The existence of the inner domain causes the value of f_∞ and ω_* to be large and the value of $\dot{p}_{a\infty}$ small, in comparison with the case without the inner domain. The effect of ponding depth on the infiltration seems to cause f_∞ in $h_w = 12$ cm to be a little bit smaller than when $h_w = 2$ cm (Exp-I(3)). Furthermore, the pore-air pressure increases with

Table 2 Same as Table 1 (type-II).

Exp-II	Sand of inner domain	L_i (cm)	f_∞ (cm/sec) $\times 10^{-3}$	ω_* (cm/sec) $\times 10^{-3}$	$\dot{p}_{a\infty}$ (cmAq/sec) $\times 10^{-3}$
(1)	K-5	9.5	3.6	9.6	3.1
(2)	K-5	23	2.9	7.7	1.3
(3)	K-5	48	3.3	9.2	1.8
(4)	K-5	48	3.3	9.6	2.3
(5)	K-5	75	2.4	7.0	1.7
(6)	K-6	75	3.0	8.3	1.4

increasing ponding depth linearly.

(2) **Type-II**

In the six cases shown in **Table 2**, the diameter of the inner domain is 2.7 cm in all cases and L_i means the depth of the inner domain. The ponding depth in all cases is about 2 cm. The changes of infiltration rate, depth of wetting front and pore-air pressure with time are shown in **Fig. 4** (1) and (2), corresponding to Exp-II(5) and (4), respectively. The arrow in the figures indicates the time, t_j, when the wetting front nearly reaches the depth of the lower boundary (bottom) of the inner domain. The following summarizes these figures, similar figures for other cases and observation during experiments.

♯1 Just after the wetting front, moving downwards through the outer domain, reaches the depth of the lower boundary of the inner domain, the infiltration rate and the pore-air pressure abruptly decreases and increases, respectively. These abrupt changes continue for a time, then become moderate.

♯2 The duration during which the abrupt change appears, $t_j^*-t_j$, becomes short with increasing depth of the inner domain. This duration is referred to as "the transition stage".

♯3 As time goes by, the infiltration rate, the velocity of the wetting front and the increasing rate of pore-air pressure tend to become constant, f_∞, ω_* and $\dot{p}_{a\infty}$, respectively (**Table 2**).

♯4 Before the wetting front reaches the depth (level) of the lower boundary of the inner domain, the variation of pore-air pressure is quitetlarge. However, after reaching the boundary, its variation becomes small.

♯5 The situation of air escape is, of course, the same as in (1) before the wetting front reaches the depth of the lower boundary of the inner domain. However, just after the arrival of the wetting front to the depth of the boundary, the escape of air from the inner domain stops and there is no escape from the sand surface. Although some time later, pore-air does escape, it is intermittent and only from the surface of the outer domain. The place of air escape seems to affect the degree of magnitude of variation of pore-air pressure mentioned in ♯4.

Table 2 reveals that according to increasing depth of the inner domain, f_∞ and

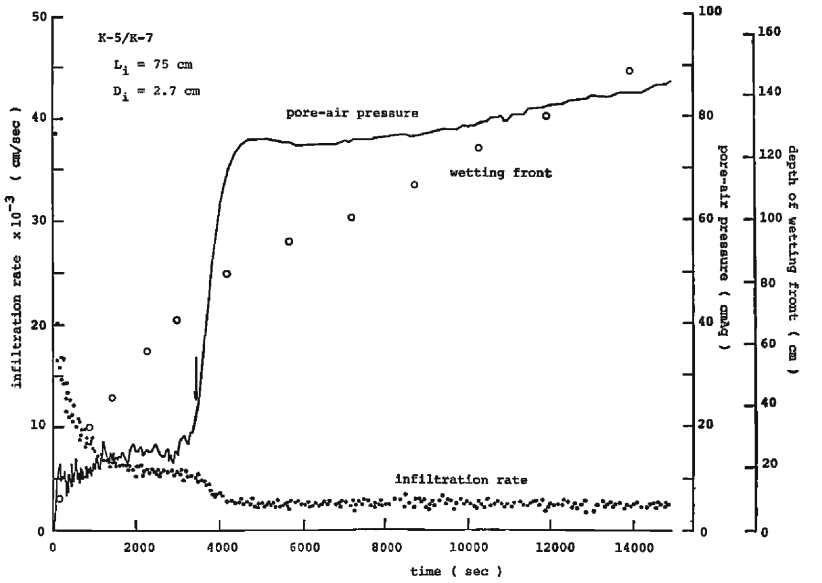

(1) L_i=75 cm

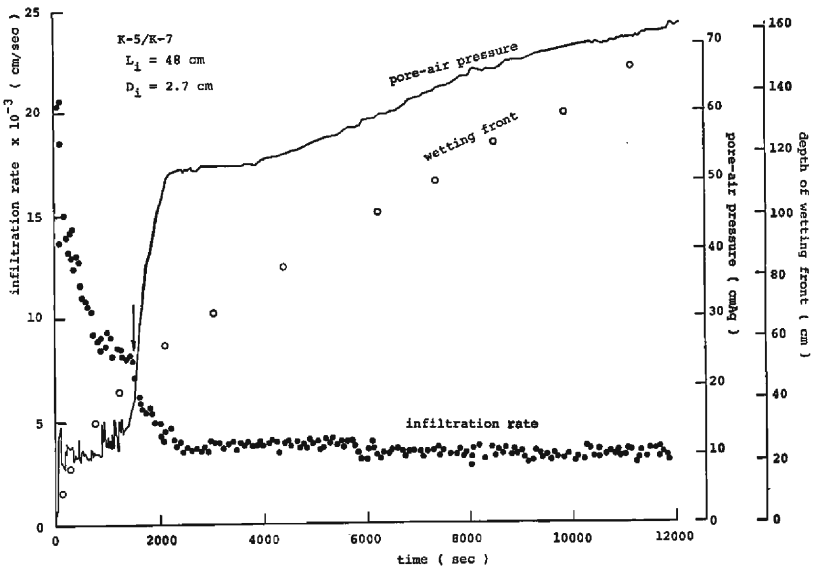

(2) L_i=48 cm

Fig. 4 Same as Fig. 2, but in the case that the inner domain breaks.

ω_* become small. And f_∞ and ω_* in type-II are smaller than those of type-I. $\dot{p}_{a\infty}$ in type-II is larger than that in type-I (**Table 1**).

Fig. 5 shows the relation between the increment of pore-air pressure, Δp_a, during the transition stage mentioned in ♯2 and the depth of the inner domain, L_i, where black and white circles are in the case of K-5/K-7 and K-6/K-7, respectively. Δp_a in

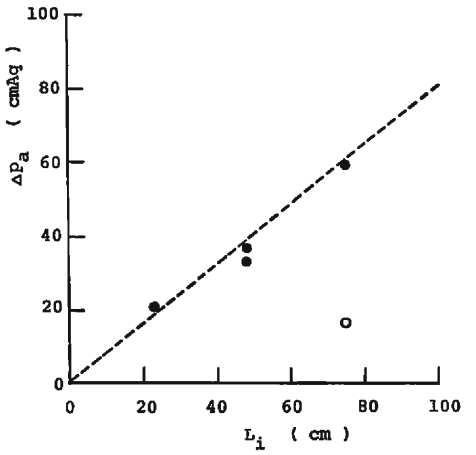

Fig. 5 Relation between Δp_a and L_i.

K-5/K-7 seems to increase linearly with L_i as shown by the broken line ($\Delta p_a \approx 0.8 L_i$), and Δp_a in K-5/K-7 is larger than that in K-6/K-7 for a fixed L_i.

3.2 Analysis

Since, as mentioned in **3.1**, the escape of pore-air into the atmosphere occurs intermittently, the infiltration phenomenon is, strictly speaking, not continuous. However, such a situation also occurs in ponded infiltration into a homogeneous sand column where we successfully treat the infiltration process as continuous[13),14)]. In similar fashion, let us assume that the infiltration process considered here can be also treated as continuous.

(1) Fundamental equation

(a) Unsaturated zone

Let us consider that, as a first approximation, water and air move vertically. Therefore, we can treat these flows one-dimensionally.

Continuity equation :

The continuity equation of water is given by

$$\frac{\partial \theta_j}{\partial t}+\frac{\partial v_j}{\partial x}=0, \quad : j=i,\ o \qquad \cdots\cdots(1)$$

where θ_j is the volumetric water content, v_j the filter velocity of water, t time, x the depth from the surface of the infiltration field, and the suffix $j=$"i" and $j=$"o" mean the quantity in the inner and the outer domains, respectively.

Let us define the following operator, $\langle\ \rangle$.

$$\langle F\rangle=(1-\sigma)F_o+\sigma F_i, \qquad \cdots\cdots(2)$$

where F is an arbitrary physical quantity. This operator repretents the cross-sectional average of F in the infiltration domain. From Eq.(1) and Eq.(2), the following equation is obtained.

$$\frac{\partial\langle\theta\rangle}{\partial t}+\frac{\partial\langle v\rangle}{\partial x}=0 \quad (3)$$

When the conditions,

$$(1-\sigma)\theta_o \gg \sigma\theta_i \quad (4)$$

and

$$1 \gg \sigma \quad (5)$$

are satisfied, Eq.(3) can be approximated by

$$\frac{\partial\theta_o}{\partial t}+\frac{\partial\langle v\rangle}{\partial x}=0. \quad (6)$$

The continuity equation of pore-air can be written by an expression like Eq. (6). However, since such a equation is not directly used later, we do not show the equation.

Equation of motion :

The movement of water and pore-air in the unsaturated zone can be expressed by the generalized Darcy's law, that is,

$$v_j=-D_j\frac{\partial\theta_j}{\partial x}+K_j\left(1-\frac{\partial p_{aj}}{\partial x}\right) \quad (7)$$

and

$$v_{aj}=-K_{aj}\frac{\partial p_{aj}}{\partial x}, \quad (8)$$

respectively, where v_{aj} is the filter velocity of air, D_j the moisture diffusivity, K_j the hydraulic conductivity, K_{aj} the permeability of air, p_{aj} the excess air pressure from the atmospheric pressure. Since the field is considered to be in the process of wetting from a dry condition, the hysteresis effect is not included in Eq.(7). While in Eq.(8), the gravitational term is neglected being much smaller than the pressure gradient term.

Operating $\langle\ \rangle$ to Eq. (8) yields

$$\langle v_a\rangle=-\langle K_a\rangle\cdot(1+\xi^*)\frac{\partial p_{ao}}{\partial x}, \quad (9)$$

where

$$\xi^*=\frac{\sigma K_{ai}}{\langle K_a\rangle}\varepsilon_p \quad (10)$$

and

$$\varepsilon_p=\left(\frac{\partial p_{ai}}{\partial x}-\frac{\partial p_{ao}}{\partial x}\right)\Big/\frac{\partial p_{ao}}{\partial x}. \quad (11)$$

Operating $\langle\ \rangle$ to Eq. (7) and introducing Eq. (9) to the equation yields

$$\langle v\rangle=\langle K\rangle(1-\tilde{A})-(1-\tilde{A})\left\langle D\frac{\partial\theta}{\partial x}\right\rangle, \quad (12)$$

where

$$\tilde{A}=\frac{r\{\langle K\rangle+\sigma K_i\varepsilon_p\}}{(1+\xi^*)\langle K_a\rangle+r\{\langle K\rangle+\sigma K_i\varepsilon_p\}} \quad \cdots\cdots(13)$$

and

$$r=-\frac{\langle v_a\rangle}{\langle v\rangle}. \quad \cdots\cdots(14)$$

When the following approximate conditions are satisfied

$$r=1, \quad \cdots\cdots(15)$$

$$\varepsilon_p=0, \quad \cdots\cdots(16)$$

$$\xi^*=0 \quad \cdots\cdots(17)$$

and

$$\frac{\partial\theta_i}{\partial x}=0, \quad \cdots\cdots(18)$$

Eq. (12) can be approximated by

$$\langle v\rangle=(1-A)\left\{\langle K\rangle-(1-\sigma)D_o\frac{\partial\theta_o}{\partial x}\right\}, \quad \cdots\cdots(19)$$

where

$$A=\frac{\langle K\rangle}{\langle K\rangle+\langle K_a\rangle}. \quad \cdots\cdots(20)$$

Furthermore, when Eq. (5) is satisfied, Eq. (19) is approximately given by

$$\langle v\rangle=(1-A)\left\{\langle K\rangle-D_o\frac{\partial\theta_o}{\partial x}\right\}. \quad \cdots\cdots(21)$$

Therefore, after substituting Eq. (21) into Eq. (6) under the condition of Eq. (4), we obtain

$$\frac{\partial\theta_o}{\partial t}=\frac{\partial}{\partial x}\left\{D_o(1-A)\frac{\partial\theta_o}{\partial x}-\langle K\rangle(1-A)\right\}. \quad \cdots\cdots(22)$$

(b) Quasi-saturated zone

In ponded infiltration into a homogeneous sand column, the movement of water and air in the quasi-saturated zone developing from the sand surface downward can be approximately expressed by an equation similar to Darcy's law[13]. The expression is not in a differential form but an integal form with respect to the total quasi-saturated zone. If the movement of both phases can be approximately expressed by the differential form in the field considered now, the filter velocity of water and air, i. e., ϑ_j and ϑ_{aj}, is given by

$$\vartheta_j=-\hat{K}_j\left(1-\frac{\partial p_{wj}}{\partial x}\right) \quad \cdots\cdots(23)$$

and

$$\vartheta_{aj}=-\hat{K}_{aj}\frac{\partial p_{aj}}{\partial x}, \quad \cdots\cdots(24)$$

where $\hat{K}_j$ and $\hat{K}_{aj}$ correspond to the hydraulic conductivity and the permeability of air in the generalized Darcy's law, respectively, p_{wj} the water pressure, and "$\wedge$" indicates the quantity in the quasi-saturated zone.

(2) Analysis in the case of type-I

(a) Quasi-saturated zone

Let us examine the situation of the development of the quasi-saturated zone in the case of type-I after time has sufficiently elapsed. The pore-air at this stage intermittently escapes from the surface of the inner domain, as mentioned in **3.1**(1) ♯5.

i) Inner domain

Integrating Eqs. (23) and (24) with $j=i$, with respect to x between $x=0$ and $x=x_{si}$ yields

$$\hat{v}_i=\hat{K}_i\left\{1-\frac{p_{wi}^{(1)}-p_{wi}^{(0)}}{x_{si}}\right\} \quad \cdots\cdots(25)$$

and

$$\hat{v}_{ai}=-\hat{K}_{ai}\frac{p_{ai}^{(1)}-p_{ai}^{(0)}}{x_{si}} \quad \cdots\cdots(26)$$

where

$$p_{wi}^{(1)}=\psi_i^{(1)}+p_{ai}^{(1)} \quad \cdots\cdots(27)$$

x_{si} is the depth of quasi-saturated zone in the inner domain, the suffix (1) and (0) mean the values at $x=x_{si}$ and $x=0$, respectively, and $\hat{K}_i$ and $\hat{K}_{ai}$ are assumed to be constant. $\psi_i^{(1)}$ corresponds to the capillary potential.

Since the pore-air escapes from the surface of the inner domain, $p_{wi}^{(0)}$ and $p_{ai}^{(0)}$ may be estimated by using the ponding depth, h_w, as[13]

$$p_{wi}^{(0)}\approx h_w \quad \cdots\cdots(28)$$

$$p_{ai}^{(0)}\approx h_w \quad \cdots\cdots(29)$$

After eliminating $p_{ai}^{(1)}$ from Eqs. (25), (26) and Eq. (27) and substituting Eqs. (28) and (29) into that, we obtain

$$x_{si}=-\frac{\alpha_i\hat{K}_i\psi_i^{(1)}}{\hat{v}_i-\alpha_i\hat{K}_i}, \quad \cdots\cdots(30)$$

where

$$\alpha_i=\frac{\hat{K}_{ai}}{\hat{K}_{ai}+r_i\hat{K}_i} \quad \cdots\cdots(31)$$

and

$$r_i=-\frac{\hat{v}_{ai}}{\hat{v}_i} \quad \cdots\cdots(32)$$

In order to clarify the developing situation of the quasi-saturated zone in the inner domain through Eq. (30), let us examine $\hat{v}_i$ and α_i included in the equation.

$\hat{v}_i$: By referring to the experimental evidence a) mentioned in **Appendix A.2**(1) that the direction of water streamline near the sand surface becomes perfectly vertical,

from Eq. (23) we obtain

$$\frac{\vartheta_i}{\vartheta_o}=\frac{\hat{K}_i}{\hat{K}_o}. \quad \cdots\cdots(33)$$

Since the infiltration rate, f, is given by

$$f=\langle v\rangle \quad \cdots\cdots(34)$$

from Eqs. (33) and (34), ϑ_i is expressed by

$$\vartheta_i=\frac{f}{\sigma+(1-\sigma)\hat{K}_o/\hat{K}_i}=\frac{fK_i}{\langle\hat{K}\rangle}. \quad \cdots\cdots(35)$$

α_i : At the stage considered now, the following relation is approximately satisfied[13].

$$f=-\sigma\vartheta_{ai} \quad \cdots\cdots(36)$$

This relation means that the infiltration rate is nearly equal to the escaping rate of pore-air. From Eqs. (35) and (36), α_i defined in Eq. (31) is expressed by

$$\alpha_i=\frac{\hat{K}_{ai}}{\hat{K}_{ai}+\langle\hat{K}\rangle/\sigma}. \quad \cdots\cdots(37)$$

r_i is as follows.

$$r_i=\langle\hat{K}\rangle/\sigma\hat{K}_i. \quad \cdots\cdots(38)$$

Now, by substituting Eqs. (35) and (37) into Eq. (30), the depth of the quasi-saturated zone in the inner domain is expressed by

$$x_{si}=-\frac{\alpha_i\langle\hat{K}\rangle\psi_i^{(1)}}{f-\dfrac{\langle\hat{K}\rangle}{1+\langle\hat{K}\rangle/\sigma\hat{K}_{ai}}}. \quad \cdots\cdots(39)$$

If the quasi-saturated zone in the inner domain does not continuously develop, that is, the degree of development is limited, the following condition must be satisfied because $x_{si}>0$ and $\psi_i^{(1)}<0$.

$$\frac{f}{\hat{K}_o}>\frac{1-\sigma+\sigma\hat{K}_i/\hat{K}_o}{1+\hat{K}_i/\hat{K}_{ai}\cdot\left(1+\dfrac{1-\sigma}{\sigma}\dfrac{\hat{K}_o}{\hat{K}_i}\right)} \quad \cdots\cdots(40)$$

$$\approx\frac{1+\sigma\hat{K}_i/\hat{K}_o}{1+\hat{K}_i/\hat{K}_{ai}\left(1+\dfrac{1}{\sigma}\dfrac{\hat{K}_o}{\hat{K}_i}\right)} \quad \cdots\cdots(40)_1$$

Let us examine x_{si} in our experiment by using Eq. $(40)_1$. The function on the right hand side of Eq. $(40)_1$ shows that, when $\hat{K}_i/\hat{K}_{ai}$ is held to be constant, the value of the function increases according to the increase of $\sigma\hat{K}_i/\hat{K}_o$. The value of $\hat{K}_i/\hat{K}_{ai}$ is given to be about 2.3. The sand approximately satisfies the following relation[13].

$$\hat{K}_j=\gamma K_{sat\,j}=\gamma Cd_j^2 \quad ;j=i,\ o \quad \cdots\cdots(41)$$

where $K_{sat\,j}$ is the saturated hydraulic conductivity and d_j the average diameter of sand. Therefore, $\hat{K}_i/\hat{K}_o$ is estimated by $\hat{K}_i/\hat{K}_o=(d_i/d_o)^2=16$ and 4 in K-5/K-7 and in K-6/K-7, respectively, where $d_j(j=o,\ i)$ is the mean diameter of sand (see : **Fig. 1**), $\gamma\approx 0.8$ and

C is constant. Since the maximum value of σ is 0.021 (in the case of $D_i=2.7$ cm), the maximum value of $\sigma\hat{K}_i/\hat{K}_o$ is 0.34 in K-5/K-7 and 0.084 in K-6/K-7. Thereby, the calculated values of the right hand side of Eq. $(40)_1$ when $\sigma\hat{K}_i/\hat{K}_o=0.34$ and 0.084 are 0.13 and 0.035, respectively. On the other hand, it is known from **Table 1** that the minimum value of $f_\infty/\hat{K}_o$ is 0.77 in K-5/K-7 ($D_i=1$ cm) and 0.75 in K-6/K-7 ($D_i=1$ cm). The comparison between these values means that our experiments satisfy the condition of Eq. $(40)_1$. After all, we can conclude that the development of quasi-saturated zone in the inner domain in the case of type-I is limited.

The quasi-saturated zone in the ponded infiltration into a homogeneous sand layer is known not to develop continuously[13]. By referring to such evidence and also by considering that the escape of pore-air occurs from the surface of the inner domain, the conclusion that the development of the quasi-saturated zone in the inner domain is limited is reasonable.

ii) Outer domain

We denote the depth of the quasi-saturated zone in the outer domain by x_{so}. Focusing on the domain between $x=x_{si}$ and $x=x_{so}$, let us first examine x_{so} under the condition that x_{si} is not very large, as mentioned above, and that $x_{so}>x_{si}$ (**Fig. 6**). Since the filter velocity of water in the quasi-saturated zone of the outer domain, ϑ_o, is, at least, affected by the inflow from the inner domain phenomenologically (experimental evidence a) in **Appendix A.2**(1)), ϑ_o is, strictly speaking, not constant with respect to the depth but increases with increasing depth under the condition that the water content in the quasi-saturated zone is constant. Let us formally rewrite Eq. (23) with $j=$"o" by using the pore-air pressure as

$$\vartheta_o=\hat{K}_o\left\{1-\frac{\partial\psi_o}{\partial x}-\frac{\partial p_{ao}}{\partial x}\right\}, \quad \cdots\cdots(42)$$

where

$$\psi_o=p_{wo}-p_{ao} \quad \cdots\cdots(43)$$

and $\hat{K}_o$ is considered to be constant. On the other hand, v_{ai} is considered to be constant, i.e. being independent of x, but K_{ai} is not constant and increases with depth due to the situation of wetness of the unsaturated zone of the inner domain. Since $\partial p_{ao}/\partial x$ for $x_{si}\leq x\leq x_{so}$ may be substituted by $\partial p_{ai}/\partial x$, from Eqs. (42) and (8) we obtain

$$\frac{\partial x}{\partial\psi_o}=1/\left\{1-\frac{\vartheta_o}{\hat{K}_o}+\frac{v_{ai}}{K_{ai}}\right\} \quad \cdots\cdots(44)$$

Integrating Eq. (44) with respect to ψ_o between $\psi_o=\psi_{si}$ and $\psi_o=\psi_{so}$ yields

$$x_{so}-x_{si}=\int_{\psi_{si}}^{\psi_{so}}\frac{1}{1-\frac{\vartheta_o}{\hat{K}_o}+\frac{v_{ai}}{K_{ai}}}d\psi_o, \quad \cdots\cdots(45)$$

where ψ_{so} and ψ_{si} mean ψ_o at $x=x_{so}$ and $x=x_{si}$, respectively. If x_{so} increases with time, the denominator of the integrand in Eq. (45) becomes zero at some ψ_o. Considering that $\partial x/\partial\psi_o\leq 0$, such a ψ_o is expected to appear at $x=x_{so}$. That is,

$$1-\frac{\vartheta_o}{\hat{K}_o}+\frac{v_{ai}}{K_{ai}}\to 0 \qquad \text{at } x=x_{so}. \qquad \cdots\cdots(46)$$

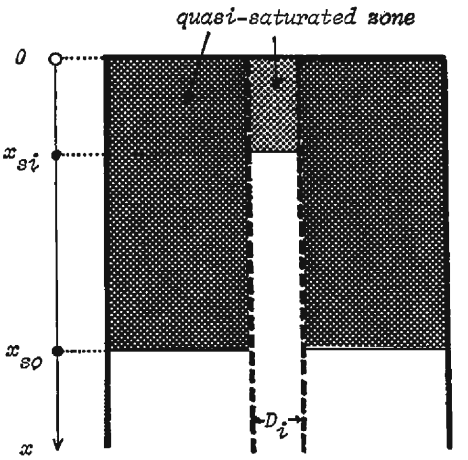

Fig. 6 Developing situation of the quasi-saturated zone.

(b) Ultimate infiltration rate

Next let us examine the infiltration rate at the stage when the condition of Eq. (46) is approximately satisfied.

Since v_i at $x=x_{so}$ can be approximated zero, the following relation is approximately satisfied from Eq. (34).

$$\{v_o\}_{x=x_{so}}=\frac{f}{1-\sigma} \qquad \cdots\cdots(47)$$

Combining Eqs. (36), (47) with Eq. (46) yields

$$f=\frac{\hat{K}_o}{\dfrac{1}{1-\sigma}+\dfrac{1}{\sigma}\dfrac{\hat{K}_o}{\{K_{ai}\}_{x=x_{so}}}}. \qquad \cdots\cdots(48)$$

θ_i at $x=x_{so}$ can be considered to be zero. Therefore, by considering the relation of Eq. (41) the permeability of air at $x=x_{so}$ is given by

$$\{K_{ai}\}_{x=x_{so}}=\frac{\mu_w}{\mu_a}\{K_{sat}\}_i=\frac{\mu_w}{\mu_a}Cd_i^2, \qquad \cdots\cdots(49)$$

where μ_w and μ_a are the viscosity coefficient of water and air, respectively. Combining the relations, Eq. (41) and Eq. (49) with Eq. (48) yields

$$\frac{\hat{K}_o}{f}=\frac{1}{1-\sigma}+\frac{\gamma}{\sigma}\frac{(d_o/d_i)^2}{\mu_w/\mu_a}(\equiv F). \qquad \cdots\cdots(50)$$

Let us denote the right hand side of Eq. (50) by F. Eq. (50) shows that the ultimate infiltration rate, f_∞, is expressed by the function of σ and $(d_o/d_i)^2$, and that the infiltration rate is independent of the ponding depth, h_∞.

i) The relation between f_∞ and σ

Since f in Eq. (50) is consistent with f_∞, let us add the suffix "∞" to f in Eq. (50). Partially differentiating $\hat{K}_o/f_\infty$ given by Eq. (50) with respect to σ yields

$$\frac{\partial \hat{K}_o/f_\infty}{\partial \sigma}=\frac{1}{(1-\sigma)^2}-\frac{\gamma}{\sigma}\frac{(d_o/d_i)^2}{\mu_w/\mu_a}. \quad \cdots\cdots(51)$$

Therefore,

$$\frac{\partial f_\infty}{\partial \sigma}\gtreqless 0 \quad \text{for } \sigma\gtreqless\sigma_*, \quad \cdots\cdots(52)$$

where

$$\frac{\sigma_*}{1-\sigma_*}=\sqrt{\frac{\gamma}{\mu_w/\mu_a}}\cdot\frac{d_o}{d_i}. \quad \cdots\cdots(53)$$

Eq. (52) shows that, if the cross-sectional area of the inner domain occupying the total infiltrating area is smaller than some value (σ_*), the ultimate infiltration rate will increase as the inner domain becomes larger.

ii) The relation between f_∞ and d_i

Partially differentiating Eq. (50) with respect to d_i yields

$$\frac{\partial \hat{K}_o/f_\infty}{\partial d_i}=-\frac{2\gamma}{\sigma d_i}\cdot\frac{(d_o/d_i)^2}{\mu_w/\mu_a}. \quad \cdots\cdots(54)$$

So, we obtain

$$\frac{\partial f_\infty}{\partial d_i}>0. \quad \cdots\cdots(55)$$

Eq. (55) means that the ultimate infiltration rate increases as the sand of the inner domain becomes coarse.

iii) The examination of experimental results

Fig. 7 shows the change of F defind in Eq. (50) against σ, where $d_o/d_i=1/2$ and $1/4$, corresponding to the case of K-6/K-7 and K-5/K-7, respectively, and the value of $\hat{K}_o$, corresponding to Sand K-7, is 5.2 x 10^{-3}cm/sec[13]. The minimum of F, i.e., the maximum of f, appears at $\sigma=\sigma_*$ defined in Eq. (53). The value of σ_* is 0.029 for $d_o/d_i=1/4$ and 0.057 for $d_o/d_i=1/2$. The value of σ in our experiment satisfies the condition that $\sigma<\sigma_*$(**Table 1**). The value of f is estimated from **Fig. 7** or Eq(50) by giving the value of d_o/d_i and σ. The value estimated from this figure, f_{es}, is shown in **Table 1.** It is seen from this table that the value of f_{es} is nearly equal to that observed for f_∞, excluding the case of $D_i=1$ cm of K-6/K-7 (Exp-1(2)). On the other hand, our experimental result satisfies the relation of Eq. (55). Therefore, we can conclude that the quasi-saturated zone in the outer domain develops continuously with time in contrast to the limited development of such a zone in the inner domain. And also we may say that the analysis mentioned above is reasonable. The ultimate infiltration rate is theoretically determined regardless of the magnitude of ponding depth as shown in Eq. (50). However, as mentioned in **3.1**(1), in our experiment, the ultimate infiltration rate at $h_w=12$ cm is a little bit smaller than that at $h_w=2$ cm. At present, the reason for such a difference is not clear.

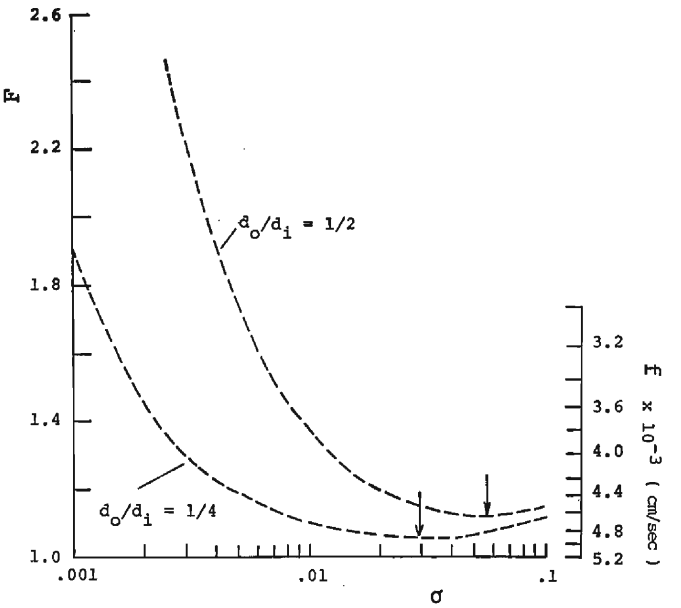

Fig. 7 Relation between F or f and σ.

The range in which F increases with σ is shown in **Fig. 7.** Since it is difficult to understand physically the relation under the condition that the quasi-saturated zone in the inner domain does not keep developing, the appearance of the range is considered to be caused by the condition of the limitation of development. By referring to the result mentioned in **Appendix** that a preferential flow in the inner domain occurs according to the increase of D_f(corresponding to D_i), i. e., σ, the physical meaning of σ_* may be considered as a kind of the criterion of σ (a necessary condition) whether the preferential flow occurs or not in the inner domain.

(c) Unsaturated zone

We will still consider the stage after an experimental time has sufficiently elapsed.

The water content in the inner domain, θ_i near the wetting front existing in the outer domain is considered to be quite small by referring to the experimental evidence c) in **Appendix A. 2**(1). Therefore, in that domain Eq. (22) is at least satisfied. By considering the experimental result mentioned in **3. 1**(1), let us assume that the wetting front comes to move downwards with an unchangeable profile and a constant veiocity, ω_*, with elapsed time. Additionally, the condition of unchangeable profile is plausible[13),14)] though the experimental evidence is not shown in this paper.

Although, as clarified in (b) iii), the quasi-saturated zone in the outer domain in our experiments continuously develops with time, to obtain a more general mathematical result we may also analyse the infiltration in the unsaturated zone in the case where the development of the quasi-saturated zone is limited.

i) The case when the quasi-saturated zone in the outer domain continuously develops

Let us assume that the developing veiocity of the quasi-saturated zone in the outer

with domain, dx_{so}/dt, becomes constant with time. This assumption will be clarified later. We also assume that $\omega_* > dx_{so}/dt$.

At the stage considered now, the following condition is satisfied or is expected to be satisfied.

1) The depth of the wetting front from the lower boundary of the quasi-saturated zone in the outer domain is very large, because $\omega_* > dx_{so}/dt$.

2) When the water content in the upper boundary of wetting front is denoted by θ_{o*}, $\partial\theta_o/\partial x = 0$ is approximately satisfied at $\theta_o = \theta_{o*}$.

3) If the water content of the quasi-saturated zone in the outer domain is denoted by θ_{om}, $\theta_i = 0$ is satisfied even at the depth where $\theta_o = \theta_{om-}$.

Moisture profile :

If we consider Eq. (22) in the domain, $\theta_{o*} - \Delta > \theta_o > 0$ (initial condition) by using the moving coordinate accompanying the advancement of the wetting front, ω_*, we obtain the following profile of the wetting front[13].

$$x - x_{o*}^{\Delta} = -\int_{\theta_o}^{\theta_{o*}-\Delta} \frac{D_o(1-A)}{\langle K\rangle(1-A) - \theta_o\omega_*} d\theta_o, \quad \cdots\cdots (56)$$

where Δ is a small positive quantity and x_{o*} means the value of x at $\theta_o = \theta_{o*} - \Delta$.

Since the denominator of the integrand in Eq. (56) must approach zero at some water content, θ_{o*} is given by

$$\theta_{o*} = \theta'_{oc}, \quad \cdots\cdots (57)$$

where θ'_{oc} is the value of θ_o at which $\langle K\rangle(1-A)/\theta_o$ shows a maximum value (**Fig. 8**).

From Eq. (57), the velocity of the wetting front is given by[13]

$$\omega_* = \left\{\frac{K_o(1-A)}{\theta_o}\right\}_{\theta_o = \theta'_{oc}}. \quad \cdots\cdots (58)$$

By considering the condition 1) mentioned above, the profile of water content between $\theta_o = \theta_{om-}$ and $\theta_o = \theta_{o*} + \Delta$ is sufficiently lengthened. In such a zone, the diffusive term on the right hand side of Eq. (22) is negligible compared to the gravitational term.

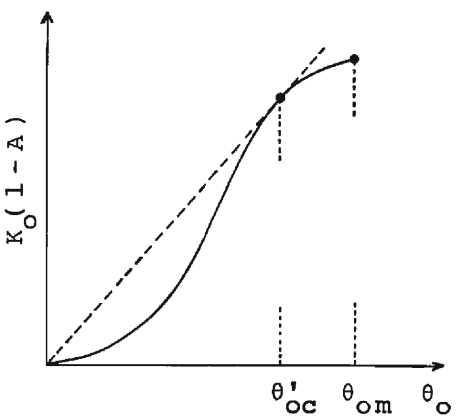

Fig. 8 Relation between $K_o(1-A)$ and θ_o.

The following equation approximates Eq. (22)[13].

$$\left(\frac{\partial x}{\partial t}\right)_{\theta_o}=\frac{d}{d\theta_o}\left\{K_o(1-A)\right\}. \quad \cdots\cdots(59)$$

Since the physical condition,

$$\left(\frac{\partial x}{\partial t}\right)_{\theta_{om-}}=\frac{dx_{so}}{dt} \quad \cdots\cdots(60)$$

must be satisfied, the sign of $dK_o(1-A)/d\theta_o$ at $\theta_o=\theta_{om-}$ is positive. This means that $dK_o(1-A)/d\theta_o$ is positive at least between $\theta_o=\theta'_{oc}$ and $\theta_o=\theta_{om}$ as shown in **Fig. 8.**

Infiltration rate :

An ultimate infiltration rate, f, is given by the right hand side of Eq. (21) at $\theta_o=\theta_{om-}$. $\frac{\partial\theta_o}{\partial x}$ at $\theta_o=\theta_{om-}$ becomes zero with time because $\frac{\partial}{\partial\theta_o}\left(\frac{\partial x}{\partial t}\right)=\frac{d^2}{d\theta_o^2}K_o(1-A)<0$ for $\theta'_{oc}<\theta_o<\theta_{om}$. Therefore, the ultimate infiltration rate is given by

$$f_\infty=\{K_o(1-A)\}_{\theta_o=\theta_{om}}. \quad \cdots\cdots(61)$$

Pore-air pressure :

The changing rate of observed pore-air pressure with time, dp_{aL}/dt can be estimated through the development of the profile of water content. Roughly speaking, the change of pore-air pressure with time is mainly determined by the development of the wetting front and the quasi-saturated zone in the outer domain given by Eq. (58) and Eq. (60), respectively. By considering Eq. (8) and Eq. (37), dp_{aL}/dt approaches the following constant, $\dot{p}_{a\infty}$ asymptotically with time.

$$\left(\omega_*-\frac{dx_{so}}{dt}\right)A'_{oc}<\dot{p}_{a\infty}<\left(\omega_*-\frac{dx_{so}}{dt}\right)A'_{oc}+\frac{f_\infty}{\sigma[K_a]_i}\cdot\frac{dx_{so}}{dt}, \quad \cdots\cdots(62)$$

where $[K_a]_i$ is the value of K_{ai} at $\theta_i=0$ and the suffix "$_c$" signifies the value at $\theta_o=\theta'_{oc}$.

Especially, when the condition, $\omega_*\gg dx_{so}/dt$ is satisfied, $\dot{p}_{a\infty}$ is approximated by

$$\dot{p}_{a\infty}=\omega_* A'_{oc} \quad \cdots\cdots(62)_1$$

ii) The case when the quasi-saturated zone in the outer domain does not continue to develop

Let us consider the case where the development of the quasi-saturated zones in the inner and outer domains are bounded at a finite depth. The wetting front, of course, continues to advance with time, so it is obvious that the profile of the water content is lengthened at some water content, θ_{o*}, where the filter velocity of water in the unsaturated zone given by Eq. (21) can be expressed by $\{\langle K\rangle(1-A)\}_{\theta_o=\theta_{o*}}$. θ_{o*} means the maximum, i. e., the water content at the upper boundary of the wetting front. The profile of the wetting front is also given by Eq. (56), and θ_{o*} and θ_{om} are determined as follows :

Two kinds of function $K_o(1-A)$, as shown in **Fig. 9**(1) and (2), may be a posteriori considered, where θ_{oc} is the θ_o at which $K_o(1-A)$ shows a maximum. In the case of **Fig. 9**(1), the following relation can be easily obtained.

$$f_\infty=\{K_o(1-A)\}_{\theta_0=\theta_{oc}} \quad \cdots\cdots(63)$$

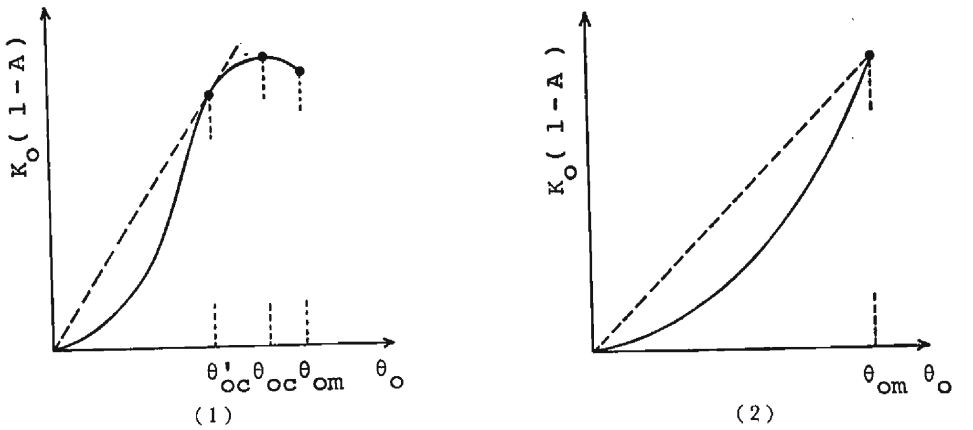

Fig. 9 Same as Fig. 8.

$$\omega_* = \{K_o(1-A)/\theta_o\}_{\theta_o=\theta'_{oc}} \quad \cdots\cdots (64)$$

$$\dot{p}_{a\infty} = \omega_* \frac{f_\infty}{\sigma}[K_a]_i \quad \cdots\cdots (65)$$

The profile of the water content ahead of the quasi-saturated zone in the outer domain is, in order of depth, composed of the zone of $\theta_{om} \geq \theta_o > \theta_{oc}$ where the shape of the profile is kept constant, the elongating zone of $\theta_{oc} > \theta_o > \theta'_{oc}$ and the wetting front. The constitution is same as in the homogeneous sand column[13].

On the other hand, in the case of **Fig. 9**(2), the following relation is satisfied.

$$f_\infty = \{K_o(1-A)\}_{\theta_o=\theta_{om}} \quad \cdots\cdots (66)$$

$$\omega_* = \frac{f_\infty}{\theta_{om}} \quad \cdots\cdots (67)$$

$$\dot{p}_{a\infty} = \omega_* \frac{f_\infty}{\sigma}[K_a]_i \quad \cdots\cdots (68)$$

The relations, Eqs. (66) and (67) are similar to unconfined infiltration into a homogeneous layer (Philip (1958)[15]).

Formally, we can also consider the pattern shown in **Fig. 8** as the shape of $K_o(1-A)$. However, this case is not possible because of the inconsistency between the velocity of the quasi-saturated zone, $dx_{so}/dt = 0$ and $\frac{\partial x}{\partial t} = \frac{d}{d\theta_o}\{K_o(1-A)\}_{\theta_{om}-} \neq 0$.

iii) Examination of the experimental results

Our experimental condition is consistent with case i) given above.

In our experiment, A defined in Eq. (20) can be approximated by $K_o/(K_o+\sigma K_{ai})$. By using this approximation let us examine the right hand side of Eq. (61), $K_o(1-A)$ for our experimental condition. The calculated value, f'_{es} is shown in **Table 1.** It is known from this table that the value of f'_{es} is fairly consistent with the observed value, f_∞, and also the value obtained in (1), f_{es}, excluding the case of Exp-I(2).

Since, as a first approximation, $\omega_* \gg dx_{so}/dt$ and $\theta'_{oc} \approx \theta_{o*} \approx \theta_{oc}$ are satisfied in our

experiment, after combining Eq. $(62)_1$ and Eq. (58), we obtain

$$\langle K_a\rangle_c \approx \omega_*^2 \theta_{o*}/\dot{p}_{a\infty}, \quad \cdots\cdots (69)$$

where the subscript "c" signifies the value at $\theta_o=\theta_{oc}$. The value of the right hand side of Eq. (69) calculated with observed values of ω_*, θ_* ($\approx\theta_{o*}$) and $\dot{p}_{a\infty}$ is shown in **Table 1.** The calculated value of $\langle K_a\rangle_c$ under $\theta_{oc}=\theta_{o*}$ and $\theta_i=0$ is also shown in the same table, where the value of θ_{o*} is used as the observed one (θ_*). Both values are in good agreement. This consistency means that our consideration is reasonable.

Based on the situation of the development of the observed profile of water content as shown in **Fig. 3**, the discussion above is undertaken under the condition that $\omega_* \gg dx_{so}/dt$. Although we can theoretically analyze the infiltration under the condition that $\omega_*=dx_{so}/dt$, that analysis is not undertaken here.

(3) Analysis in the case of type-II

(a) Infiltration situation during the transition stage, $t_j<t<t_j^*$

i) Quasi-saturated zone

At first, let us focus on the stage just before the wetting front moving downwards in the outer domain reaches the depth of the inner domain. The escape of pore-air at this stage appears from the surface of the inner domain. By integrating Eq. (23), the velocity of water in the quasi-saturated zone in the outer domain is given by

$$\hat{v}_o \approx \hat{K}_o\left\{1-\frac{\phi_o^{(1)}+p_{ao}^{(1)}-p_{wo}^{(1)}}{x_{so}}\right\} \quad \cdots\cdots (70)$$

where

$$p_{wo}^{(1)}=\phi_o^{(1)}+p_{ao}^{(1)} \quad \cdots\cdots (71)$$

and

$$p_{wo}^{(0)}=h_w \quad \cdots\cdots (72)$$

The symbol "nearly equal" in Eq. (70) is based on the fact that the water-flow from the inner to the outer domains occurs, as mentioned previously. $\phi_o^{(1)}$ can be considered to be consistent with the water entry value in the outer domain, ϕ_{ao} as a first approximation. If we intend to calculate the right hand side of Eq. (70), the estimation of $p_{ao}^{(1)}$ is necessary. However, it is difficult to estimate the value directly. So, let us use two methods to estimate $p_{ao}^{(1)}$. The one is to approximate $p_{ao}^{(1)}$ by the air pressure measured at the bottom of the sand column. The other is to approximate by the pore-air pressure at the lower end of the quasi-saturated zone in the inner domain, $p_{ai}^{(1)}$. The value of $p_{ao}^{(1)}$ is, in fact, expected to exist between the values found by the above two approximations. The latter is as follows : Combining Eqs. (25) and (26) and using the conditions, Eqs. (28) and (29) yield

$$p_{ai}^{(1)} \approx (1-\alpha_i)x_{si}-(1-\alpha_i)\phi_i^{(1)}+h_w \quad \cdots\cdots (73)$$

$(1-\alpha_i)$ on the right hand side of Eq. (73) is estimated as follows : r_i defined in Eq. (32) satisfies the condition that $r_i \gg 1$. If we consider the case that $\sigma \to 1$, i. e., the case of the homogeneous sand column, r_i becomes unity approximately and α_i defined in Eq.

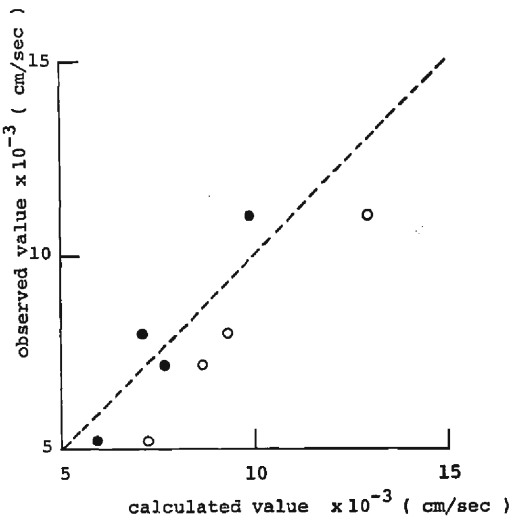

Fig. 10 Comparison between the observed and the calculated infiltration rates.

(37) is approximately about 0.3[13] (Eq. (81)). Therefore, by taking account of these conditions, $(1-\alpha_i)$ in the present case is approximated by unity. **Fig. 10** shows the relation between the observed infiltration rate at $t=t_j$ and the calculated value of the right hand side of Eq. (70), where black and white circles correspond to the values estimated by the former and latter approximations respectively. The broken line shown in the figure is a straight line with the slope of 45° passing through the origin. In the calculation x_{so} is approximated by x_{so} at $t=t_j^*$, mentioned in the next section (b), and in the latter calculation x_{si} and $\phi_i^{(1)}$ are approximated by zero and the air entry value, respectively. It is known from this figure that the infiltration rates calculated are fairly consistent with the observed one. Therefore, by considering that x_{so} at $t=t_j$ in the calculation, is approximated by x_{so}^* at $t=t_j^*$, we may expect that the development of a quasi-saturated zone in the outer domain during the transition stage is not much.

ii) Pore-air pressure

Next, let us examine the increment of pore-air pressure observed during the transi-

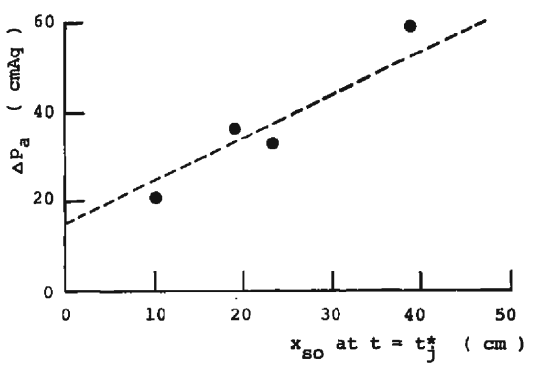

Fig. 11 Relation between Δp_a and x_{so} at $t=t_j^*$.

tion stage, Δp_a, shown in **Fig. 5. Fig. 11** shows the relation between Δp_a and x_{so} at $t=t_j^*$ in the case of K-5/K-7, where the value of $x_{so}(t_j^*)$ is estimated later. It is known from this figure that the experimental data, Δp_a is approximately expressed by the following function

$$\Delta p_a = x_{so}(t_j^*) + 15 \ \text{(cmAq)}, \quad \cdots\cdots (74)$$

where the broken line in the figure shows the function.

Although the graph of $x_{so}(t_j^*)$ against L_i is not shown here, the following relation is satisfied.

$$x_{so}(t_j^*) \approx \frac{L_i}{\kappa} \quad ; \kappa = 2 \quad \cdots\cdots (75)$$

Now let us consider the reason why Eq. (74) is satisfied. From Eq. (73) the pore-air pressure at the bottom of sand column, p_{aL} at $t=t_j$ is expressed by

$$p_{aL}(t_j) \approx A_o x_{si}(t_j) + A_1\{x_{so}(t_j^*) - x_{si}(t_j)\} + A_2\{L_i - x_{so}(t_j^*)\} - \psi_i^{(1)} + h_w + \tilde{p}_a(t_j), \quad \cdots (76)$$

where A_0, A_1 and A_2 are a mean pressure gradient in $0<x<x_{si}(t_j)$, $x_{si}(t_j)<x<x_{so}(t_j^*)$ and $x_{so}(t_j^*)<x<L_i$, respectively, and $\tilde{p}_a$ is the increment of pore-air pressure from $x=L_i$ to the bottom of the sand column.

On the other hand, since the escape of pore-air at $t=t_j^*$ appears from the surface of the outer domain, p_{aL} at $t=t_j^*$ is also expressed by[13]

$$p_{aL}(t_j^*) \approx A_1^* x_{so}(t_j^*) + A_2^*\{L_i - x_{so}(t_j^*)\} - \psi_{so} + h_w + \tilde{p}_a(t_j^*), \quad \cdots\cdots (77)$$

where A_1^* and A_2^* are a mean pressure gradient in $0<x<x_{so}(t_j^*)$ and $x_{so}(t_j^*)<x<L_i$, respectively, and ψ_{so} is nearly equal to the water entry value of the sand which forms the outer domain. The water entry value of Sand K-7 is about -20 cmAq[13].

If we subtract Eq. (76) from Eq. (77) and use Eq. (75), we obtain the following relation.

$$p_{aL}(t_j^*) - p_{aL}(t_j) \approx \underline{A} x_{so}(t_j^*) + \Delta\psi_e + \{\tilde{p}_a(t_j^*) - \tilde{p}_a(t_j)\} \quad \cdots\cdots (78)$$

where

$$\underline{A} = (A_1^* - A_1)(1-\eta) + (A_2^* - A_2)(\kappa - 1),$$

$$\Delta\psi_e = -\psi_{so} + \psi_i^{(1)} \quad \text{and} \quad \eta = 1 - \frac{x_{si}(t_j)}{x_{so}(t_j^*)} \cdot \frac{A_o - A_1}{A_1^* - A_1}.$$

In the right hand side of Eq. (78), $p_a(t_j^*) - p_a(t_j)$ may be neglected being insignificant in comparison with the magnitude of other terms, and η may be approximated by unity because $A_o \approx A_1^*$ and $x_{so}(t_j^*) \gg x_{si}(t_j)$. Since the left hand side of Eq. (78) is consistent with Δp_a, it is seen that Eq. (78) corresponds to Eq. (74). By using the values $\psi_i^{(1)} = -5$ cmAq (the air entry value of Sand K-5, ref. **Fig. 15**) and $\psi_{so} = -20$ cmAq, $\Delta\psi_e$ is calculated to be about 15 cmAq. This value is known to be consistent with that shown in Eq. (74). Although $\kappa = 2$ and A is approximately given by $(A_2^* + A_1^* - A_2 - A_1)$, it is not easy to estimate the value of A because the values of A_1^*, A_1 and A_2 are not known at present. However, the following relations are satisfied. $A_2^* = (1-\alpha_{co}) \approx 0.7$ (see : section (b)), $A_2 \ll A_2^*$ and $A_1 \ll A_1^*$. Furthermore, A_1^* is considered to be much smaller than

A_2^*. Thereby, roughly speaking, we may expect that the value of A is fairly close to unity as estimated in the experiment.

After all, it can be said that the increase of pore-air pressure at the transition stage is mainly caused by the differences between the magnitude of the depth of the developed quasi-saturated zone and the magnitude of the water entry value in the outer and inner domains.

iii) Escape route of the pore-air

As mentioned in **3.1**(2) ♯5, after the wetting front advancing downwards in the outer domain reaches the depth of the inner domain, the location of the escaping pore-air changes to the surface of the outer domain. This experimental evidence is phenomenologically explained as follows. If we refer to the flow situation of water in the outer domain shown in **Appendix A.2**(2) a), it may be supposed that after the portion of the penetrating water moving through the outer domain near the inner domain reaches the depth of the inner domain, that portion of water starts to move under the bottom of the inner domain. Furthermore, we may also suppose that the inner domain becomes saturated, excluding entrapped air, due to the penetrating water throughout the inner domain. However, if the sand of the inner domain close to the boundary of its domain is saturated, the sand in the outer domain close to the boundary of the inner domain is also saturated because of the difference of soil-water characteristic curves of both sands. The wetness of the sand surrounding the inner domain caused by these phemonena seals the previous escape route of pore-air. As a result, the new escape route through the outer domain, having less resistance in comparison with the previous one, is formed.

(b) The ultimate development of the quasi-saturated zone in the outer domain

The flow rate of water in the inner domain after the arrival of the wetting front to the depth (level) of the lower boundary of the inner domain is expected to be still sufficiently smaller than in the outer domain. Therefore, by considering that the pore-air escapes from the surface of the outer domain, the following approximate equation is satisfied.

$$f=-(1-\sigma)\vartheta_{ao}=(1-\sigma)\vartheta_o \quad \cdots\cdots(79)$$

By combining Eq. (79) with Eqs. (25) and (26) with $i=$"o" and referring to the reduction of Eq. (30), we obtain the following approximate equation for x_{so}.

$$x_{so}=-\alpha_{co}\frac{\hat{K}_o\psi_{eo}/(1-\alpha_{co})}{f-\alpha_{co}\hat{K}_o} \quad \cdots\cdots(80)$$

where ψ_{eo} is the water entry value in the outer domain and α_{co} is defined as follows[13].

$$\alpha_{co}=\frac{\hat{K}_{ao}}{\hat{K}_{ao}+\hat{K}_o} \quad \cdots\cdots(81)$$

Let us examine situation of the development of the quasi-saturated zone in the outer domain at $t=t_f^*$ and $t=t_\infty$, where t_∞ indicates a sufficiently long time. When we insert the values of infiltration rate observed at $t=t_f^*$ and $t=t_\infty$ into the right side of Eq. (80), we obtain the relation shown in **Fig. 12**, where black and white circles represent

the case of K-5/K-7 and K-6/K-7, respectively, and $\alpha_{co}=0.28$[13], $\psi_{ao}=-20$ cmAq and $\hat{K}_o=5.2\times10^{-3}$ cm/sec as used above. It appears that, in this figure, the calculated values are described by two broken straight lines, C-I and C-II, of which the border is 20 cm, where C-II has a slope of 45°. The value of 20 cm corresponds to the ultimate depth of the quasi-saturated zone in ponded infiltration into the homogeneous sand column of Sand K-7[13]. By considering the escape situation of pore-air and the

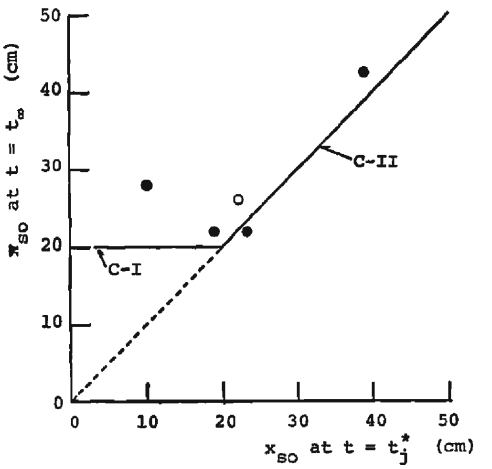

Fig. 12 Relation between the values of x_{ao} at $t=t_j$ and $t=t_\infty$.

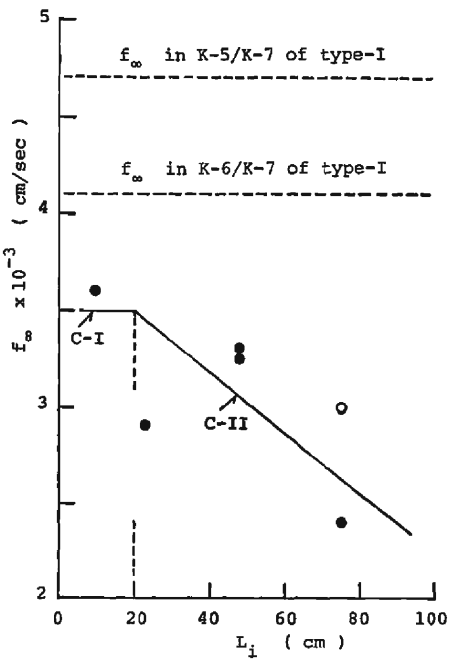

Fig. 13 Relation between f_∞ and L_i.

result mentioned in (a) that the development of quasi-saturated zone in the outer domain is small during the transition stage, it is reasonable, as a first approximation, to consider that the quasi-saturated zone in the outer domain can develop to $x_{so}=20$ cm in the case of $x_{so}(t_j)<20$ cm and the quasi-saturated zone in the case of $x_{so}(t_j)>20$ cm does not develop any more for $t>t_j^*$.

Experimentally, the depth of the quasi-saturated zone which developed in the outer domain in the case of $x_{so}(t_j)>20$ cm was less than that of the inner domain. And as seen in (a) iii), the outer domain close to the inner domain is saturated. Although the above indicates that the condition of water flow in the outer domain of $x<L_i$ is not uniform for the lateral direction, the degree of the non-uniformity of water flow may be supposed to be close to the cross-sectional average.

(c) Ultimate infiltration rate

Fig. 13 shows the relation between the ultimate infiltration rate and depth of inner domain (**Table 2**), where two broken lines, C-I, C-II and circles correspond to those in **Fig. 12.** The value of 3.5×10^{-3} cm/sec is the ultimate infiltration rate in a ponded infiltration into the homogeneous layer of Sand K-7 (**Table 1**). The changing situation of the ultimate infiltration rate against the depth of the inner domain corresponds to that in **Fig. 12.** In fact, we know from **Fig. 4** that the degree of decrease of infiltration rate for $t>t_j^*$ is large in the case of a shallow inner domain, but the degree in a deep inner domain is small. The degree of decrease corresponds to that of the development of quasi-saturated zone in $t>t_j$ mentioned in (b).

As assumed in the beginning of the this section, the analysis undertaken above is based on the condition that the infiltration process not being continuous may be treated as being continuous on the average. Finally, through the discussion above, we may say that underlying conditions in the analysis are plausible.

4. Flux infiltration

4.1 Experimental results

Fig. 14(1), (2) and (3) show the changes of infiltration rate, depth of wetting front and pore-air pressure with time, where q is the rate of water supply on the surface of the infiltration field (rainfall intensity). All of the infiltration fields in this flux condition are K-5/K-7. From these figures, the figures in other cases (**Table 3**) and the detailed observation during experiments, the following results have been obtained.

♯1 At a relatively early stage before ponding on the sand surface, the pore-air pressure linearly increases with time, except at the stage just after the beginning time of the experiment, but after some time ($t=t^*$) the pressure begins to increase abruptly. Subsequently, while the abrupt increase of pore-air pressure macroscopically appears, the situation that after the rate of increase of pore-air pressure becomes small, the rate of change temporarily becomes zero was microscopically observed. The time when the rate of change of the pressure shows zero is fairly consistent with the ponding time, t^{**}. The degree of the increase in $t^{**}>t>t^*$ becomes large as the rainfall becomes strong.

#2 The pore-air pressure, on the average, continues increasing remarkably through the ponding time. The situation of the surface of the infiltration field just before and just after ponding is as follows. During the abrupt increase of pore-air pressure, a small air bubble escapes from the surface of both the outer and inner domains, accompanied by a sound like breaking with a click. Some time later, the top surface of the

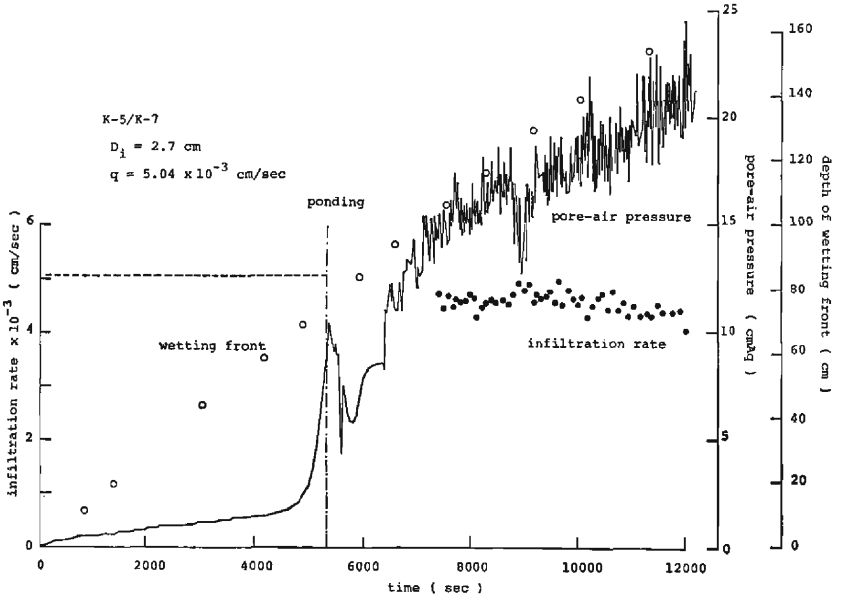

(1) $q=5.04\times10^{-3}$cm/sec in $D_i=2.7$ cm.

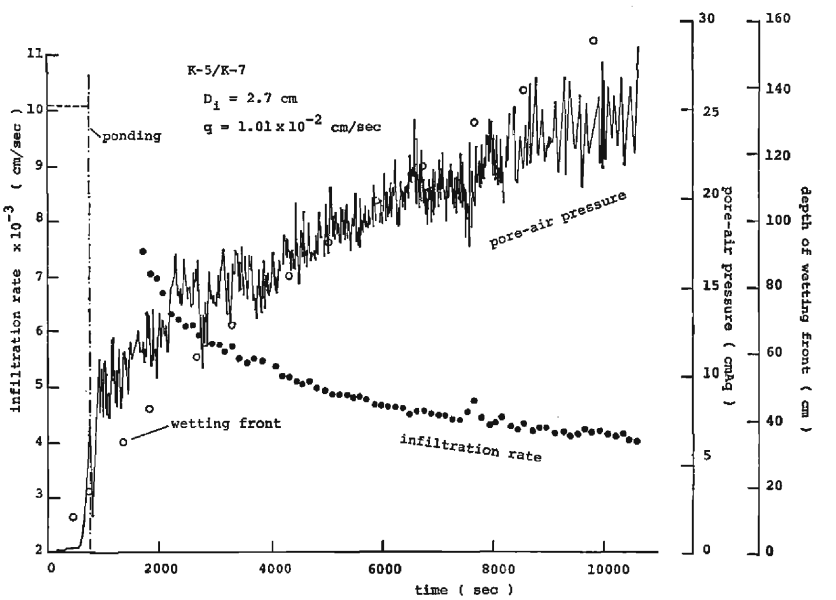

(2) $q=1.01\times10^{-2}$cm/sec in $D_i=2.7$ cm.

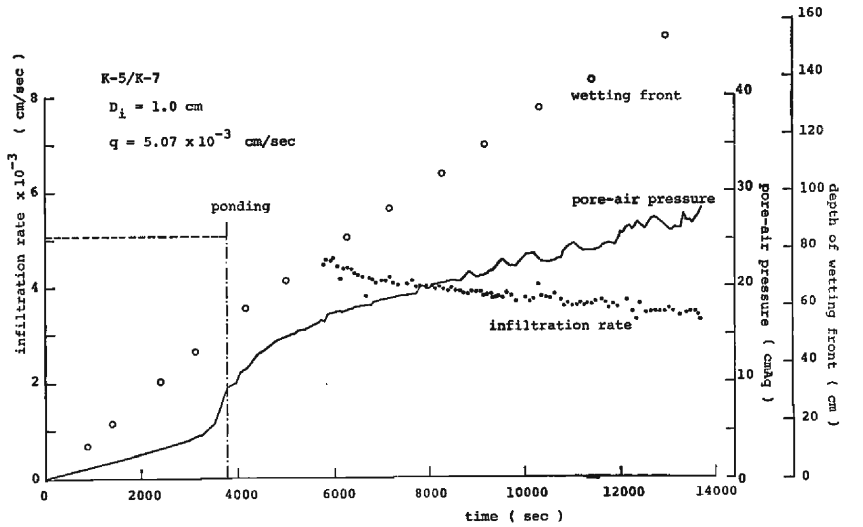

(3) $q=5.07\times10^{-3}$cm/sec in $D_i=1$ cm.

Fig. 14 Same as Fig. 2, but in the flux infiltration.

inner domain swells and then returns to its original level, accompanied witht he escape of a relatively large air bubble. At that instant the pore-air pressure abruptly falls. Subsequently, the escape of pore-air intermittently appears only from the surface of the inner domain, and the pore-air pressure increases with time, accompanied by a remarkable repeated rise and drop.

#3 The wetting front in the outer domain advances with about a constant velocity before ponding, but after ponding, its velocity gradually decreases and then becomes constant, ω_* with time. The asymptotic value seems to be independent of rainfall

Table 3 Same as Table 1, but in the flux infiltration (type-I).

	D_i (cm)	r (cm/sec) $\times10^{-3}$	f_∞ (cm/sec) $\times10^{-3}$	ω_* (cm/sec) $\times10^{-2}$	θ_*	$\dot{p}_{a\infty}$ $\times10^{-3}$
1	1	5.07	3.5	0.97	0.37	1.33
2	1	4.27	3.8		0.39	
3	1	4.00			0.39	
4	2.7	19.8	4.0	1.2	0.39	
5	2.7	19.7	(4.8)	1.3	0.39	
6	2.7	10.1	(4.1)	1.2	0.39	
7	2.7	7.5	3.9	1.1		
8	2.7	7.5	4.2	1.3	0.37	
9	2.7	5.04	4.4	1.2	0.37	
10	2.7	4.75	4.1	1.2	0.37	
11	2.7	4.50			0.38	

( ) : infiltration rate still decreases

intensity (**Table 3**).

♯4 After ponding occurs, the infiltration rate continuously decreases and approaches a constant value, f_∞, asymptotically. The asymptotic value seems to be also independent of rainfall intensity (**Table 3**).

4.2 Discussion

(1) Stage before ponding occurs

Let us express the quantity at $t=t^*$ and $t=t^{**}$ by using the mark "*" and "**", respectively. **Fig. 15** shows the relation between the pore-air pressure, p_{aL} and the depth of wetting front in the outer domain, x_f at $t=t^*$ and $t=t^{**}$, where black squares and black circles mean the values at $t=t^*$ and $t=t^{**}$ in the case of $D_i=2.7$ cm, respectively, and white circles mean the values at $t=t^*$ in the case of $D_i=1$ cm. The value of p_{aL}^* when $D_i=2.7$ cm seems to be about 1.5 cmAq regardless of the magnitude of rainfall intensity, though such a situation does not appear when $D_i=1$ cm. The value of p_{aL}^{**} when $D_i=2.7$ cm seems to increase with x_f^{**} as shown by a broken line in the figure. The value of p_{aL}^{**} on the line at $x_f^{**}=0$ is about 5 cmAq. This value corresponds to the air entry value of Sand K-5 which forms the inner domain. So, the inner domain near the surface is expected to be nearly saturated at $t=t^{**}$, and the abrupt increase of air pressure after $t=t^*$ is obviously caused by the formation of large resistance to the escape of pore-air. If we consider the relation between the abrupt increase of the air pressure and the formation of the quasi-saturated zone clarified in the flux infiltration into a homogeneous sand column[14], we may say that the formation of large resistance corresponds to the formation of the quasi-saturated zone. Because the air

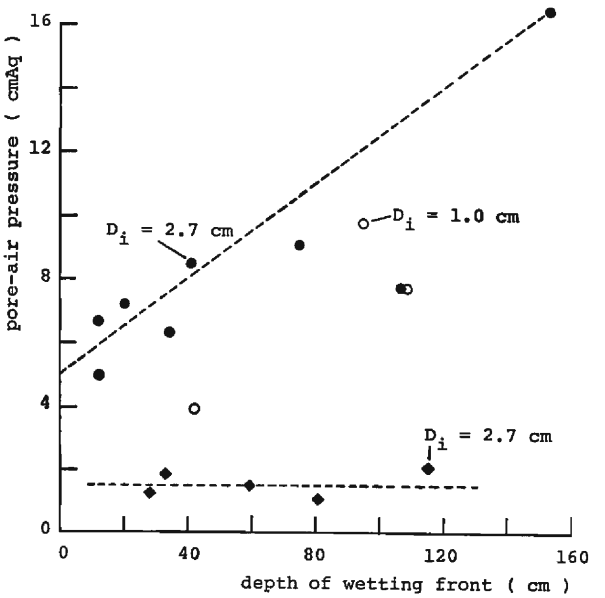

Fig. 15 Relation between the pore-air pressure and the depth of wetting front at $t=t^*$and $t=t^{**}$.

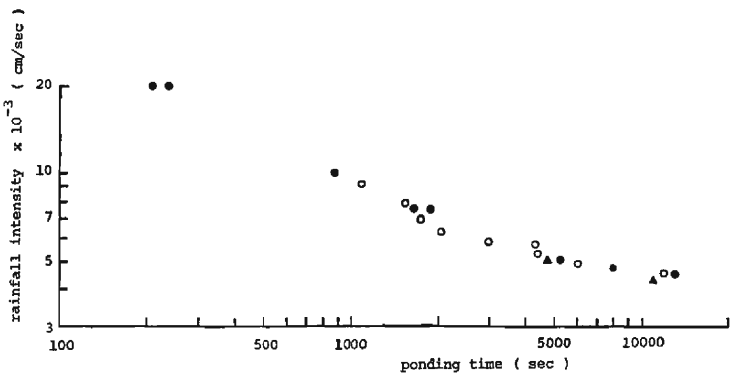

Fig. 16 Relation between the ponding time and the rainfall intensity.

pressure is measured at the lower end of the sand column and the escaping air encounters a resistance through the unsaturated zone in the sand column, p_{aL}^{**} increases as x_f^{**} increases.

Fig. 16 shows the relation between the ponding time and the rainfall intensity, where black circles and triangles are for the cases of $D_i=2.7$ cm and $D_i=1$ cm, respectively. The white circles in the figure are for the case of a homogeneous sand column. **Fig. 17** shows the relation between the depth of wetting front at the ponding time and the rainfall intensity. The symbols used are the same as in **Fig. 16.** Experimental results show that as the diameter of the inner domain increases, the ponding time becomes long and the wetting front at the ponding time becomes deep. And also, as the degree of heterogeneity due to the inner domain decreases, the relations shown in **Figs. 16** and **17** seem to approach those for the case of a homogeneous sand column.

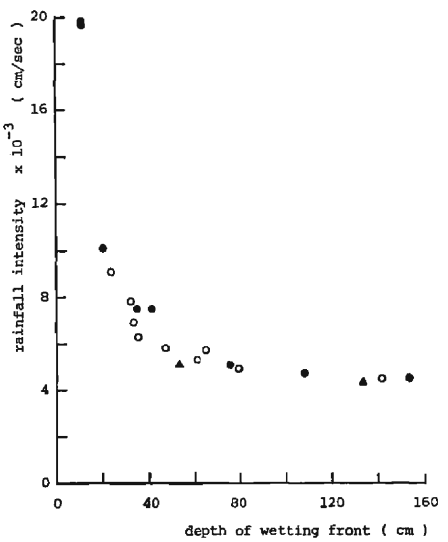

Fig. 17 Relation between the depth of wetting front at the ponding time and the rainfall intensity.

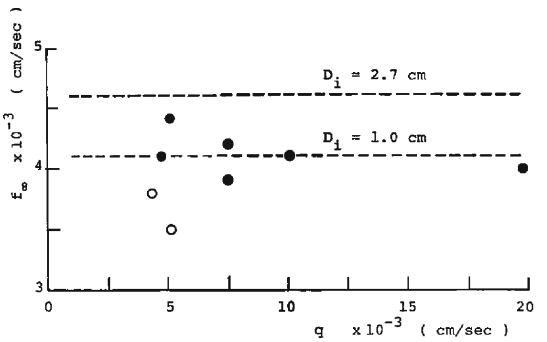

Fig. 18 Relation between the ultimate infiltration rate and rainfall intensity.

In fact, the degree of difference between graphs for the homogeneous and the heterogeneous sand columns is originally not large.

The fundamental equations expressing the heterogeneous sand columns, Eq. (21) and Eq. (22) are not essentially different from those of the homogeneous sand column, because the procedure of $\sigma \to 0$ lets the fundamental equations of the heterogeneous sand column simplify to those of the homogeneous one. Therefore, the ponding time or the depth of wetting front at the ponding time may be theoretically estimated, if the method already shown in our paper[14] is applied to Eqs. (21) and (22).

(2) Stage after ponding occurs

Fig. 18 shows the relation between the ultimate infiltration rate and the rainfall intensity, where black and white circles represent the case of $D_i = 2.7$ cm and $D_i = 1$ cm, respectively. The two broken lines in this figure show the value of ultimate infiltration rate in ponded infiltration for $D_i = 2.7$ cm and $D_i = 1$ cm with K-5/K-7 (**Table 1**). The ultimate infiltration rate into a homogeneous sand column of Sand K-7 is about 3.5×10^{-3} cm/sec. It is understood from this figure that the ultimate infiltration rate in flux infiltration is a little bit smaller than that in ponded infiltration. As the ultimate infiltration rates in ponded and flux infiltrations into the homogeneous sand column are nearly the same[14], the present disagreement between both values is phenomenologically interesting. The reason may be considered to be as follows :

The quasi-saturated zone in the inner domain is formed in both types of infiltration (i. e., ponded and flux), and the escape of pore-air from the surface in the inner domain also occurs in both cases. However, the unsaturated zone beneath the quasi-saturated zone in flux infiltfation develops more than in ponded infiltration because the quasi-saturated zone in flux infiltration is formed later than in the ponded infiltration. Therefore, the resistance against air movement through a sand column in flux infiltration is larger than that in ponded infiltration. Furthermore, if we, in practice, consider the situation through Eq. (61), the increase in the resistance is expected to correspond to the increase of A defined in Eq. (20) due to the decrease of $\langle K_a \rangle$ at $\theta_o = \theta_{om-}$. The decrease of $\langle K_a \rangle$ is expected to be based on the increase of water content at $x = x_{so-}$. As a result, the ultimate infiltration rate in flux infiltration becomes smaller than that

in ponded infiltration.

6. Conclusion

We have experimentally and analytically examined the infiltration process under ponding and flux conditions into an experimentally constructed heterogeneous sand column that consists of two concentric columns, an outer column of a homogeneous finer sand column, and a column of coarser sand. The coarser sand column is connected to the surface of the finer sand column. The two columns are referred to as the outer domain and inner domain, respectively. The following has been disclosed.

In the case where the inner domain reaches the bottom of its surrounding sand column (outer domain):

1) In ponded infiltration, until the wetting front, moving downwards through the outer domain, reaches its bottom, the pore-air intermittently escapes from the sand surface of the inner domain, but not just after the beginning of experiments.

2) The infiltration situation is similar to that into a homogeneous sand column. However, the ultimate infiltration rate is larger than that in the homogeneous sand column, and the rate increases as the diameter of the inner domain becomes large and also as the sand of the inner domain becomes coarser. The quasi-saturated zone in the outer domain continues to develop though the development of the corresponding zone in the inner domain ceases with time. Otherwise, the conditions necessary for the development of the quasi-saturated zone in the inner domain is the same as in the homogeneous sand column. The rate of advancement of the wetting front in the inner domain is much smaller, compared with the rate of the outer domain.

3) With the constant flux infiltration, as the diameter of the inner domain increases, the ponding time becomes long, though the difference between the ponding times in the homogeneous and in the heterogeneous sand columns is not necessarily large in our experiment. The ultimate infiltration rate after ponding on the surface occurs is a little bit smaller than that in the ponded infiltration because of the difference of wetness condition of the infiltration field before ponding, but the infiltration rate is larger than that in homogeneous sand column.

In the case where the inner domain does not reach the bottom of the outer domain:

4) In the ponded infiltration under the condition that the depth of the inner domain is limited, just after the wetting front in the outer domain arrives at the depth of inner domain, the escaping situation of pore-air dramatically changes. That is, the pore-air begins to escape from the surface of the outer domain after a temporary cessation of escape. Then this situation continues till the wetting front reaches the bottom of the outer domain. The change of escape-route of air is caused by the phenomenon of the inner domain becoming saturated.

5) Accompanying the change of the air escape-route, the infiltration rate and the pore-air pressure abruptly decreases and increases, respectively. The ultimate infiltration rate and the ultimate depth of the quasi-saturated zone developed in the outer domain

are determined mainly by the relation of magnitude between $x_{so}(t_j)$ and x_s^{hom}. $x_{so}(t_j)$ indicates the depth of the quasi-saturated zone in the outer domain at $t=t_j$, where t_j is the time at which the wetting front in the outer domain reaches the depth of the inner domain. x_s^{hom} indicates the ultimate depth of the quasi-saturated zone developed in the ponded infiltration into the homogeneous sand column. The value of x_s^{hom} in Sand K-7 and Sand K-6 is about 20 cm. That is, in the case where $x_s^{hom}>x_{so}(t_j)$, the quasi-saturated zone in the outer domain can develop to the ultimate depth in the homogeneous sand column and the ultimate infiltration rate becomes nearly equal to that in the homogeneous one. However, in the case where $x_s^{hom}<x_{so}(t_j)$, the quasi-saturated zone developed deeply in the outer domain after the wetting front in the outer domain reaches the depth of the inner domain can be considered, as a first approximation, not to develop any more. The ultimate infiltration rate becomes smaller than that in the homogeneous sand column and the rate decreases as the depth of the inner domain becomes large.

Although we have dealt with the simple heterogeneous infiltration field characterized by a heterogeneous sand column with a fine grained outer domain and a coarser inner domain, the extension of the result obtained in our research to the problem of a homogeneous field vertically containing regularly spaced small, coarser sand cylinders (inner domains) with the same diameter and the same depth is possible. However, the clarification of infiltration into a field where a lot of cylinders with various magnitudes of diameter and depth distributed spatially in a homogeneous layer should rely on numerical simulation and remains as a future problem.

References

1) A. J. Peck: Field Variability of Soil Physical Properties, in Advances of Irrigation, ed. by D. Hillel, Vol. 2, Academic Press, 1983, pp. 189–219.
2) Beven, K. and P. Germann: Macropores and Water Flow in Soils, Water Resou. Res. Vol. 18, 1982, pp. 1311–1325.
3) Warrick, A. W. and D. R. Nielsen: Spatial Variability of Soil Physical Properties in the Field, in Applications of Soil Physics, Academic Press, 1980, pp. 319–333.
4) Smith, R. E. and R. H. B. Hebbert: A Monte Carlo Analysis of the Hydrologic Effects of Spatial Variability of Infiltration, Water Resour. Res., Vol. 15, 1979, pp. 419–429.
5) Sharma, M. L., Gander, G. A. and G. G. Hunt: Spatial Variability of Infiltration in a Watershed, J. of Hydrol., Vol. 45, 1980, pp. 101–122.
6) Maller, R. A. and M. L. Sharma: An Analysis of Areal Infiltration Considering Spatial Variability, J. of Hydrol., Vol. 52, 1981, pp. 25–37.
7) Maller, R. A. and M. L. Sharma: Aspects of Rainfall Excess from Spatial Varying Hydrological Parameters, J. of Hydrol., Vol. 67, 1984, pp. 115–127.
8) Germann, P. and K. Beven: Water Flow in Soil Macropores, I. An Experimental Approach, J. of Soil Science, Vol. 32, 1981, pp. 1–13.
9) Germann, P. and K. Beven: Kinematic Wave Approximation to Infiltration into Soils with Sorbing Macropores, Water Resour. Res., Vol. 21, 1985, pp. 990–996.
10) Beven, K. and P. Germann: Water flow in Soil Macropores, II. A Combined Flow Model, J. of Soil Science, Vol. 32, 1981, pp. 15–29.
11) M. R. Davidson: A Green-Ampt Model of Infiltration in a Cracked Soil, Water Resour. Res., Vol. 11, 1984, pp. 1685–1690.
12) M. R. Davidson: Asymptotic Infiltration into a Soil Which Contains Cracks or Holes but Whose

Surface is Otherwise Impermeable, Transport in Porous Media, Vol. 2, 1987, pp. 165-176.
13) Ishihara, Y. and E. Shimojima: A Role of Pore-air in Infiltration Process, Bull. of Disast. Prev. Res. Inst., Kyoto Univ., Vol. 33, 1983, pp. 163-222.
14) Shimojima, E. and Y. Ishihara: Infiltration process of Rainfall with Constant Intensity, Bull. of Disast. Prev. Res. Inst., Kyoto Univ., Vol. 34, 1984, pp. 55-104.
15) J. R. Philip: The Theory of Infiltration, 6. Effect of Water Depth over Soil, Soil Sci., Vol. 85, 1958, pp278-286.

Appendix: Experiment by using a rectangular prismatic box

In the experiment using the cylinder, it is difficult to know directly the situation of water flow in the inner and the outer domains. However, the direct examination of the situation of water flow in both domains is very important to understand the infiltration process into the heterogeneous domains. Therefore, in order to overcome the difficulty, an experiment has been supplementally carried out as follows.

A. 1 Apparatus and method of the experiment

Using a transparent rectangular prismatic box, 60 cm wide, 1. 9 cm thick and 60 cm deep, the following heterogenous infiltration field is made. The field is similar to that mentioned in **2,** but two-dimensional. The inner domain of Sand K-5 in the uniform sand layer of Sand K-7 (outer domain) is vertically set in the center of the box (see: **Photo. I**). The sands employed are initially air-dried. To make the flow situation clearly visible, the powder dye, Rhydamine-B, is suitably placed at several positions of the sand layer.

The water supply into the field is controlled so that the ponding condition of about 1 cm is maintained.

During the experiments, the situation of the flow of water and the escape of pore-air into atmosphere were examined by using a video camera. The pore-air pressure near the bottom in the central part of the sand layer was measured by using a small pressure gauge of 2. 8 mm diameter and 8 mm long.

The experiment was also carried out till the wetting front reached the bottom of the layer under the same room conditions stated in **2.**

A. 2 Experimental results

(1) The case where the inner domain reaches the bottom of the field

Flow situation of water :

Photo. I(1) shows the situation of water flow in the case of the inner domain with 1. 9 cm width (D_f) at the elapsed time (t) of 18′13″, where the square lattice in the photo is 5 cm $\times$5 cm. In this case $\sigma=0.032$, and the part containing much water and little water appears as dark and light in the photo, respectively. The following is revealed from detailed observation of the video film.

a) The streamline of water in the outer domain is nearly vertical for about 2-3 cm depth. However, as the depth increases, the streamline, at first, spreads outward and then becomes vertical. The degree of spreading outward decreases as the streamline

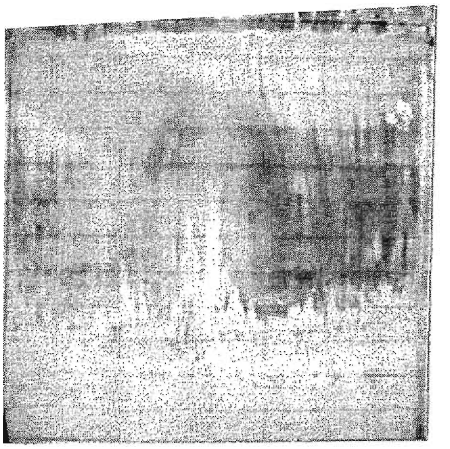

(1) $D_f = 1.9$ cm

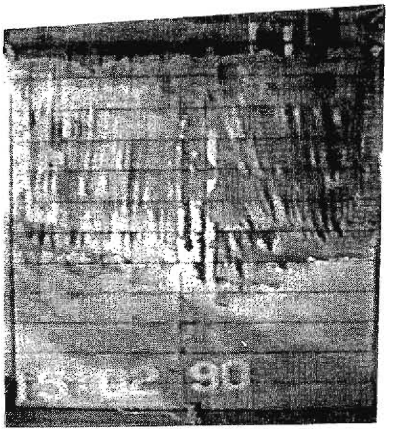

(2) $D_f = 6$ cm

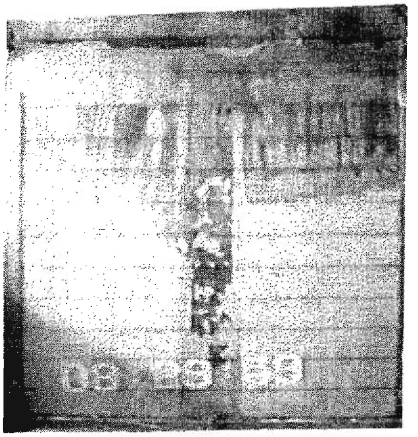

(3) $D_f = 10$ cm

Pnoto. I Flow situation of water in the case of type-I.

becomes more distant from the inner domain.

b) Excluding a situation close to the sand surface, the degree of wetness in the inner domain at a depth where the streamline spreads outward is relatively large. However, there seems to be no water in the inner domain at a depth where the streamline is vertical.

c) The condition that the streamline speads outward means that the penetrating water through the inner domain flows into the outer domain. The development of the wetting front in the outer domain is much more extensive than that of the inner domain (**Fig. I**(1)).

Photo. I(2) is the case of $D_f=6$ cm ($\sigma=0.1$) at $t=11'42''$. In the inner domain, two advancing dark lines are seen so that the inner domain is vertically divided into three parts. The lines are not the streamlines through the inner domain, but the pathlines of water on a streak of Sand K-7 attached to the wall when the inner domain was made. The following was understood from the video film.

d) The penetrating water through the inner domain does not flow uniformly, being different from the case of $D_f=1.9$ cm, with some part advancing ahead of others. But the movement of advancing flow does not continue for a long time, and as soon as the wetting front reaches the side boundary of the inner domain, the movement stops for a time due to absorption by the outer domain. Then the movement starts downwards again. Such a flow pattern is cyclically repeated (**Fig. I**(2)). However, the velocity of the wetting front within the inner domain is less than that in the outer domain.

e) The streamline in the outer domain is not necessarily symmetrical with respect to the inner domain. This situation is determined by which side bnundary of the inner domain absorbs the wetting front in the inner domain.

Photo. I(3) is the case of $D_f=10$ cm ($\sigma=0.17$) at $t=7'53''$. The following is revealed from the video film.

f) After some time, the wetting front in the inner domain starts to move down with a very large velocity (**Fig. I**(3)). And the magnitude of the velocity is much larger than that in the outer domain. Let us denote the flow situation in the inner domain as "preferential flow". This preferential flow seems to advance without cease, being different from the flow situation in the case of $D_f=6$ cm.

Advancement of the wetting front, change of the pore-air pressure and escape of the pore-air :

Fig. I(1), (2) and (3) show the changes of the depth of the wetting front and the air pressure with time, corresponding to **Photo. I**(1), (2) and (3), respectively, where black and white circles represent the depths of wetting front in the outer and inner domains, respectively. As the shape of the wetting front is, as usual, not horizontal, the position of the wetting front is decided by mean depth. The following results were obtained from these figures and also from the observation of the video film.

g) When the pore-air pressure violently varies with in a short cyclic period, the escape of pore-air occurs from the surface of the inner domain. On the other hand, when the air pressure shows a relatively moderate change, the escape occurs from the surface of the outer domain.

h) As the wetting front in the outer domain advances, its velocity decreases, and then it becomes more or less constant with time. However, the wetting front in the inner domain advances stepwise and the actual advance is accompanied by an abrupt drop of air pressure, i. e., the occurrence of an air escape. Although the advancement

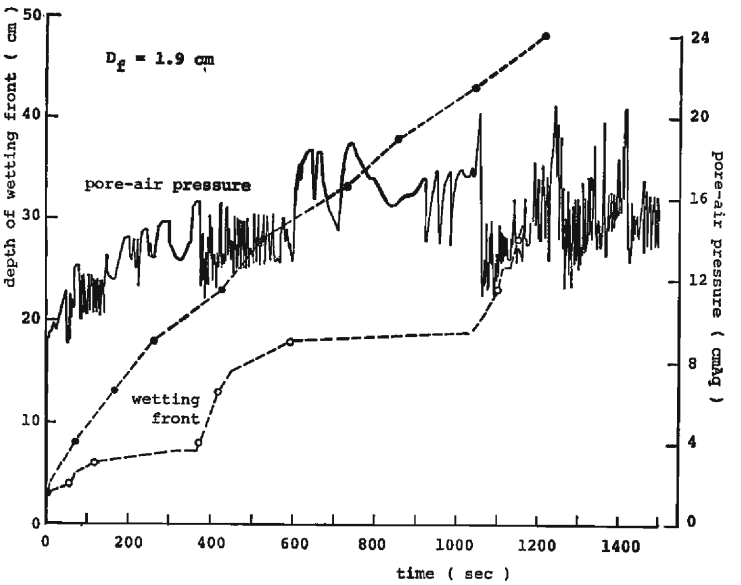

(1) D_f=1.9 cm

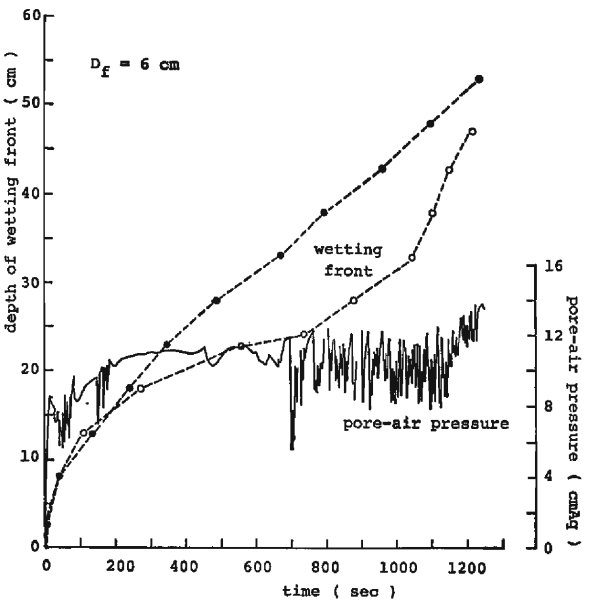

(2) D_f=6 cm

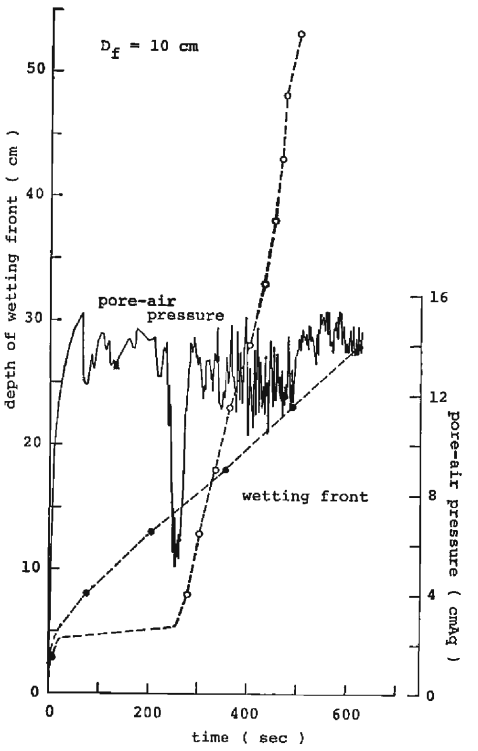

(3) $D_f=10$ cm

Fig. I Changes of the depth of wetting front and the pore-air pressure with time in the case of type-I.

of the wetting front like step is not seen in the case of $D_f=10$ cm, such a movement can be expected by the reason of the flow rate of penetrating water through the inner domain always being larger than the rate water is absorbed by the outer domain.

(2) The case where the inner domain does not reach the bottom of the field

Flow situation of water :

Photo. II shows the situation of water flow at $t=16'41''$ after the wetting front in the outer domain has reached the depth of the inner domain, in the case of $D_f=1.9$ cm ($\sigma=0.032$) and $L_i=25$ cm. The following is revealed from the video film.

a) After the arrival of the wetting front in the outer domain to the depth of the inner domain, the streamline in the outer domain near the inner domain tends to spread under the bottom of the inner domain.

b) In spite of time elapsed, the infiltration through the inner domain hardly proceeds. The orientation of the streamline in the outer domain then becomes vertical.

c) Some time later, the streamline in the outer domain begins to spread outward, accompanied by the development of wetting front in the inner domain. This is due to the occurrence of water flow from the inner to the outer domains.

Situations of the pore-air pressure and the air escaping :

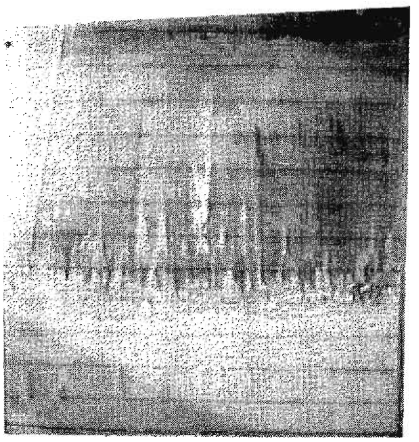

Photo. II Same as Photo. I, but in the case of type-II.

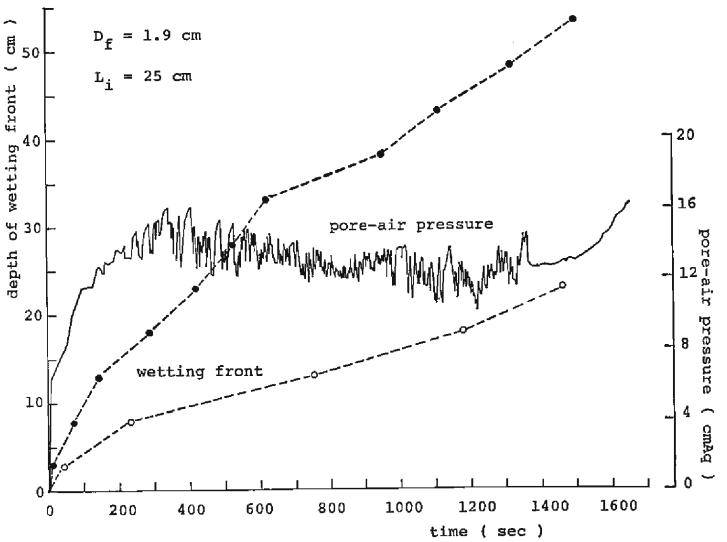

Fig. II Same as Fig. I, but in the case of type-II.

Fig. II shows the changes of the depth of wetting front and the pore-air pressure with time, with black and white circles corresponding to **Fig. I.** From this figure and the video film, the following is understood.

d) The abrupt increase of air pressure and the change of air escaped route as noted in **3.1**(2) do not appear even at stage a) and b).

e) However, when time proceeds to stage c), the air pressure starts to increase abruptly and the air escape route changes from the surface of inner domain to that of the outer domain.